Title

Identification of Functional Targets Reveals that the Suppression of Pumilio-mediated mRNA Decay Increases Cell Resistance to DNA Damage in Human Cells

Authors

Toshimichi Yamada, Naoto Imamachi, Katsutoshi Imamura, Takeshi Kawamura, Masami Nagahama, Nobuyoshi Akimitsu*

Affirmations

T.Y. and M.N.; Meiji Pharmaceutical University, Tokyo, Japan

N.I., T.K., and N.A.; Isotope Science Center, The University of Tokyo, Tokyo, Japan

K.I.; Department of Microbiology and Molecular Genetics, Graduate School of Pharmaceutical Sciences, Chiba University, Chiba, Japan

Author List Footnote

*: lead contact

Contact Infor

Correspondence: akimitsu@ric.u-tokyo.ac.jp

Summary

RNA-binding proteins (RBPs) play a pivotal role in gene expression by modulating the stability of transcripts; however, the identification of functional targets remains difficult, even for RBPs with a high specific binding ability, such as mammalian PUMILIO proteins (PUMs). To understand the role of RBPs in biological processes and diseases, we present a systematic approach to define the functional targets of an RBP and determine the stimulus that modulates RBP-mediated mRNA decay. We applied our method to investigate PUM function and identified 49 functional target mRNAs of PUM1. Moreover, *in silico* screening indicated that DNA damage reagents inhibit PUM1-mediated mRNA decay, thus enhancing cell viability. Finally, we applied our method to UPF1 and showed that UPF1-mediated mRNA decay was activated by rapamycin. Thus, our study establishes a systematic and un-biased strategy to identify the biological role of RBPs through the identification and analysis of transcripts directly regulated by RBPs.

Introduction

The ability of cells to sense environmental changes and adapt to external conditions is critical for cell survival. Tuning gene expression is crucial for cellular adaptation to environmental changes, with extensive regulation constructed by transcriptional and post-transcriptional mechanisms (López-Maury et al., 2008; Nadal et al., 2011; Spriggs et al., 2010). Cells regulate the amounts of mRNAs in response to various stimuli through the modulation of both synthesis and decay rates (Miller et al., 2011; Rabani et al., 2011, 2014). The synthesis rate of a transcript is controlled by transcription factors (TFs), whereas the decay rate is regulated by RNA-binding proteins (RBPs) and miRNAs (Hentze et al., 2018; Rabani et al., 2014). To understand the regulatory mechanisms in cellular responses to stimuli, it is important to identify the functional connection between regulators (TFs and RBPs) and their targets (DNAs and RNAs). In addition, the identification of stimuli that modulate the regulator-target pathway will indicate the biological significance of the regulator-target pathway for the adaptation to the environmental change.

Analytical frameworks have been constructed to extract the functional linkage between TFs and their target genes by integrating various high-throughput data on TF binding and gene expression (Gardner et al., 2003; Karlebach and Shamir, 2008). These frameworks have defined target genes of particular TFs by analyzing the correlation of expression between the TF and transcripts in diverse high-throughput data (Bar-Joseph et al., 2003; Hu et al., 2007; Lee et al., 2002). A positive correlation in expression between the particular TF and a set of genes in response to various stimuli indicates that the TF is a transcriptional activator. In contrast, an inverse correlation in expression between the particular TF and a set of genes with various stimuli suggests that the TF is a transcriptional repressor. Based on this idea, previous studies have indicated a specific combination of particular TFs and their targets, as well as the biological conditions/stimuli under which the TF-mediated gene expression is regulated (transcriptional activation or repression) (Segal et al., 2003). In contrast to the success in studying TFs, an analytical framework for RBPs that regulate RNA stability remains limited. Investigations of the inverse correlative expression of RBP and mRNAs have not succeeded in the identification of a functional linkage between RBPs and their target transcripts. Recently, extensive studies have been conducted in the identification of binding RNAs to particular RBPs (Dominguez et al., 2018; Nussbacher and Yeo, 2018; Wheeler et al., 2018). However, determining the function of RBPs remains difficult even though RNAs bound to RBPs have been identified. In addition, there is no systematic approach to identify the stimulus that regulates RBP-mediated mRNA degradation. A

novel approach to identify the role of RBPs in post-transcriptional regulation has been eagerly anticipated.

We present an analytical framework that combines the experimental identification of functional targets of RBPs and the computational identification of stimuli that modulate RBP-mediated gene regulation. In this study, "*bona-fide* targets" of the RBP of interest are experimentally determined as transcripts that satisfy the following two criteria: (1) a transcript bound to the RBP and (2) a transcript for which the stability is affected in the RBP-depleted cells. By applying this method, we previously identified 246 targets of UPF1 (Imamachi et al., 2016). To develop a computational pipeline that identifies the combination of stimuli and RBP-mediated gene regulation, we constructed an *in silico* screening scheme by using the publicly available RNA-seq data of human cells treated with various stimuli. If the RBP mediates the alteration of RNA expression level in response to a certain stimulus, the expression change in the RBP will be inversely correlated with that of the targets. Based on this assumption, *in silico* screening may be used to identify a stimulus that promotes or inhibits RBP-mediated mRNA decay (**Figure 1**). Overall, our method specifies the post-transcriptional regulation of particular transcripts governed by the RBP of interest under specific conditions. Our method thus generates testable hypotheses that suggest the biological roles for an RBP and the conditions under which it acts.

We applied our methodology to human PUMILIO (PUM) proteins (Miller and Olivas, 2011; Quenault et al., 2011; Wang et al., 2018), one of the most conserved family of eukaryotic RBPs. PUMs regulate target mRNAs via binding to the 5'-UGUAHAUA-3' sequence in the 3' un-translated region (3'UTR). PUM proteins are suggested to have roles in the development and neuronal system by regulating specific mRNAs (Wang et al., 2018). Considering human PUMs are ubiquitously expressed in diverse tissues, PUMs are thought to have as-yet-unknown cellular functions. Although previous genome-wide analyses have identified mRNAs that are bound to PUMs (Galgano et al., 2008; Hafner et al., 2010), *bona-fide* targets of PUMs at transcriptome level remained elusive. Furthermore, the specific stimuli that modulate PUM-mediated mRNA regulations in the cells remain unknown. Thus, defining *bona-fide* targets of PUMs and stimuli that activate/suppress PUM activity is critical for understanding the role of PUMs in both cellular function and disease.

In this study, we initially identified 49 mRNAs as *bona-fide* targets of PUM1. *In silico* screening of 481 RNA-seq data deposited on Gene Expression Omnibus (GEO) identified DNA damage agents as an inhibitory stimulus for PUM1-mediated mRNA decay. We experimentally tested this computational prediction and identified the

biological role of PUM1 in the cellular resistance to DNA damage agents. This experimental result verified the method's predictions and provided the previously uncharacterized role of PUM1. Finally, we also applied the method to another RBP, UPF1, and demonstrated that UPF1-mediated mRNA decay is promoted by a rapamycin stimulus, thus highlighting the generality of our method.

Results

Strategy to systematically study the biological function of RBP-mediated mRNA decay.

Our methodology comprises two parts: (i) the identification of *bona-fide* target mRNAs of the RBP and (ii) the identification of stimuli that regulate the RBP-mediated mRNA decay (**Figure 1**). *Bona-fide* targets of the RBP of interest are defined by two criteria. One criterion is mRNAs bound to the RBP, which are determined by RNA immunoprecipitation sequencing (RIP-seq) (Zhao et al., 2010). The other criterion is mRNAs degraded by the RBP, which are determined by 5′-bromo-uridine (BrU) immunoprecipitation chase-deep sequencing analysis (BRIC-seq) (Tani et al., 2012; Yamada et al., 2018). BRIC-seq enables the determination of genome-wide RNA stability by chasing chronological decreases of BrU-labeled RNAs under a physiologically non-disturbed condition. The RNA half-life of each transcript is calculated from the decreasing BrU-labeled RNA. By comparing the RNA half-lives between normal cells and RBP depletion cells, we can identify the mRNA for which the stability is regulated by the RBP (Imamachi et al., 2016). Merging the results of RIP-seq and BRIC-seq yields the *bona-fide* targets of the RBP (**Figure 1**). Through this analysis, we can identify the functional connection between an RBP of interest and its targets.

To investigate the biological role of the RBP, we aimed to identify external stimuli that modulate RBP-mediated mRNA decay. Our analysis is based on the following idea: If the expression levels of the RBP and its targets respond to a stimulus in an inverse-correlated manner, the stimulus is regarded as a candidate modulator (promoter or inhibitor) of RBP-mediated mRNA decay (**Figure 1**). To identify these stimuli, we developed an analytical pipeline for *in silico* screening of the massive dataset, which contains hundreds of RNA-seq profiles deposited in Gene Expression Omnibus (GEO). In this pipeline, the alteration of the expression levels of the RBP (mRNA) and its targets to stimuli is quantified by calculating the fold-change of the mRNA expression levels in each RNA-seq dataset. This pipeline enables us to systematically identify the stimuli that modulate the RBP-mediated mRNA decay, thus providing biological insights regarding RBP function.

Identification of *bona-fide* target mRNAs of human PUM1 and PUM2 by the combinatorial analysis of RIP-seq and BRIC-seq.

The human PUM family consists of two members encoded in independent genes (PUM1 and PUM2) that share 83% overall similarity, with the RNA-binding domain

(PUM-HD) being 97% similar (Spassov and Jurecic, 2002) (**Figure 2A**). PUM-HD consists of eight repeats that bind specifically to 5'-UGUAHAUA-3' (Wang et al., 2001, 2002). To identify binding mRNAs to PUMs, we applied RIP-seq to FLAG-tagged PUM1 and FLAG-tagged PUM2 with a similar over-expression level in HeLa Tet-off (TO) cells. By setting the cutoff limit for the false discovery rate at 0.05, we determined 3,097 and 2,813 mRNAs bound to PUM1 and PUM2, respectively (**Figure 2B, Table S1**). Both PUM1 and PUM2 shared most of their binding targets (2,671 mRNAs, **Figure 2C**). Moreover, the fold enrichment of the PUM1-bound mRNAs was highly correlated with that of the PUM2-bound mRNAs (R^2 = 0.97, **Figure 2D**). We confirmed the specific binding of mRNAs on FLAG-PUMs via RIP-qPCR (**Figure S1A, upper panel**). In addition, we confirmed mRNAs bound to endogenous PUMs using specific antibodies against PUM1 or PUM2 (**Figure S1A, lower panel**). Motif analysis of both PUM1 and PUM2 binding mRNAs yielded the 5'-UGUAHAUA-3' sequence, which is the typical binding motif of PUM (**Figure 2E**). These results indicate that the *in vivo* target selectivity of PUM1 and PUM2 is nearly the same.

To investigate the functional classification of the mRNAs associated with PUMs, we searched for shared Protein Analysis THrough Evolutionary Relationship (PANTHER) for the binding mRNAs. PANTHER indicated a significant enrichment of components related to developmental processes (247 mRNAs, FDR < 1.1×10^{-4}), mitosis (73 mRNAs, FDR < 1.6×10^{-3}), and the MAPK cascade (66 mRNAs, FDR < 1.7×10^{-2}) (complete results presented in **Table S2**). These enriched categories are consistent with a previous study that analyzed PUM-bound mRNAs (Galgano et al., 2008).

To analyze the effect of PUMs on mRNA decay, we measured the changes in the mRNA half-lives following the depletion of the PUM proteins (**Figure S1B**) using BRIC-seq. By comparing the altered mRNA half-lives between PUM1 and PUM2 knockdown (KD), we determined that PUM1 KD has a larger impact on the mRNA stability than PUM2 KD in HeLa TO cells (**Figure 2F**). For example, the half-life of the *ERLEC1* transcripts in PUM1 KD cells was greater than 12 hours, which was significantly longer than that in control or PUM2 KD cells (5.7 hours or 5.8 hours, respectively). In contrast, there was no effect of PUM KD for a transcript that lacked PUM motif, such as *ABCC1* mRNA. The result was quantitatively validated via BRIC-qPCR (**Figure S1C**). A genome-wide comparison of the mRNA half-lives indicated that the number of stabilized transcripts in PUM1 KD cells was greater than that in PUM2 KD cells (**Figure 2G, Table S1, Figure S1D**).

By merging the results of BRIC-seq with RIP-seq, we identified 48 transcripts that were associated with PUM1 and were significantly stabilized in PUM1 KD cells

(**Figure 2H, Table S1**). In contrast, only four transcripts in de-stabilized mRNAs by PUM1 KD were associated with PUM1, which implies that the main role of PUM1 is mRNA degradation in HeLa TO cells. In the case of PUM2, only a single transcript belonged to the intersections of RIP-seq and BRIC-seq (**Figure 2H**). We considered that these mRNAs are not *bona-fide* targets of PUM2 because the transcripts lack the PUM motif in their sequences. Thus, we defined the 48 transcripts as *bona-fide* targets of PUM1.

Qualitative and quantitative analyses of PUM1 and PUM2.

The negligible effect of PUM2 on mRNA degradation prompted us to hypothesize that PUM1, but not PUM2, recruits mRNA decay factors on the targets. To test this idea, we isolated PUM1 and PUM2 complexes and identified associated proteins using mass spectrometry. FLAG-PUM1 and FLAG-PUM2 expressed in HeLa TO cells with similar expression levels were affinity purified. Compared with the control immunoprecipitation, several bands were identified on the SDS-gel as candidates for PUM-associated proteins (**Figure S2A**). These PUM-associated proteins were analyzed via mass spectrometry with three criteria for the identification: a 1% false discovery cut off; more than three unique peptides; and at least five-fold enrichment in PUM immunoprecipitates compared to the control. With these criteria, purified PUM complexes included multiple subunits of the CCR4-NOT deadenlyase complex, including CNOT1,2,7,9 (**Figure S2B**). We subsequently confirmed the interaction between PUMs and CNOT1 using co-immunoprecipitation (**Figure S2C**). Consistent with our result, the interactions between PUMs and CNOT components have previously been identified in HEK293 cells (Etten et al., 2012). Other mRNA decay factors identified in the PUM complexes included enhancer of mRNA de-capping (EDC4) and a member of the trinucleotide repeat containing 6 protein family (TNRC6A). TNRC6A is related to gene silencing by miRNA and siRNA (Elkayam et al., 2017; Jakymiw et al., 2005; Nishi et al., 2013). Although the fold enrichment of CNOT9 was 2.7 times higher in PUM1-IP, the majority of the decay factors show similar yields between PUM1 and PUM2. Moreover, TNRC6A preferentially binds to PUM2. These binding features between PUMs and the decay factors indicated that PUM2 also has a potential to degrade mRNAs. Taken together, the interaction between PUMs and RNA decay factors is not sufficient to explain the dominant function of PUM1 in mRNA decay.

We subsequently estimated the expression ratio of endogenous PUM1 versus endogenous PUM2 using quantitative Western blot. Endogenous PUM protein signals in HeLa TO cell lysate were detected using corresponding anti-bodies. To quantitatively compare the endogenous amounts of PUM1 and PUM2, we used FLAG-PUMs as a

standard (**Figure S3A**). By normalizing the PUM band intensity with the GAPDH band and FLAG-tag band intensities visualized by Western blotting, the endogenous PUM1/PUM2 ratio was estimated as 7.1 ± 0.1 (**Figure S3B**). This ratio is similar to the value previously quantified in HCT116 cells (PUM1/PUM2 = 7.5) (Lee et al., 2016). Based on this measurement, we suppose that the difference in protein expression may explain the reason why PUM2 KD does not affect mRNA stability in HeLa TO cells, although the binding ability of PUM2 to mRNAs and RNA decay factors is nearly equivalent to that of PUM1 (**Figure 2D**, **Figure S2**). If we consider that both PUM1 and PUM2 have the same potential to control mRNAs in HeLa TO cells, the complete loss of PUM2 by RNA silencing leads to only a 13% loss of PUM proteins in the cells, which indicates that the remaining PUM proteins (PUM1) degrade mRNAs with similar kinetics to a non-silenced condition (**Figure S3C**). Thus, the negligible effect of PUM2 on mRNA degradation in HeLa TO cells may be explained by the low expression of PUM2.

Identification of DNA damage agents as inhibitors of PUM1-mediated mRNA decay.

The initial bioinformatic analysis using PANTHER did not show functional enrichment in the 48 PUM1 targets, which suggests that a novel analytical pipeline is required to investigate the biological role of PUM1-mediated mRNA decay. To this end, we developed an *in silico* screening scheme to identify a specific stimulus that influences the PUM1-mediated mRNA decay, based on the principle that the stimulus causes inverse-correlated expression changes between PUM1 and its target mRNAs. If the stimulus decreases the PUM1 level, the PUM1 targets should be increased (**Figure 3A**) and vice versa. To perform this *in silico* screening, we collected 491 RNA-seq data obtained in various stress conditions from Gene Expression Omnibus (GEO, **Table S2**). To quantify whether the overall trend of PUM1 targets is increased or decreased following a stimulus, we introduced a "variation index". This index is defined by the sum of numbers of increased and decreased PUM1 targets (**Figure 3B, also refer to Methods**). Each variation index of PUM1 targets was plotted against the corresponding log2-fold-change of PUM1 mRNA level. The data in the second and fourth quadrants in the scatterplot are the candidate stimuli that modulate the PUM1-mediated mRNA decay. In detail, a stimulus that increases PUM1 mRNA and decreases PUM1 targets is judged as a promoter of PUM1-mediated mRNA decay. In contrast, a stimulus that decreases PUM1 mRNA and increases PUM1 targets is judged as an inhibitor of PUM1-mediated mRNA decay.

For promoters of PUM1-mediated mRNA decay, ailanthone (AIL) and a mixture of Reston virus (RESTV) and lipopolysaccharide (LPS) were selected as candidates. AIL

is a potential anti-cancer drug for castration-resistant prostate cancer (CRPC) by inhibiting androgen receptor signaling (He et al., 2016). The result of the mixture of RESTV and LPS suggests the activation of PUM1-mediated mRNA decay by infections. A previous study demonstrated that PUM proteins positively regulate RIG-I-like receptor signaling, which detects invading pathogens (Narita et al., 2014). Although the previous study used Newcastle disease virus (NDV), these results suggest that PUM1 has a role in the immune response to infections of diverse pathogens.

For candidate inhibitors of PUM1-mediated mRNA decay, *in silico* screening yielded well-known anti-cancer drugs, such as trichostatin A (TSA), camptothecin (CPT), and cisplatin (CDDP), which cause DNA damage and induce apoptosis by inhibiting DNA replication and/or RNA transcription (**Figure 3C and 3D**). Although the molecular mechanism of Compound Kushen Injection (CKI), a mixture of natural compounds extracted from Kuehen and Baituling in China, remains under investigation (Wang et al., 2015), a recent study showed that the effect of CKI on gene expression is similar to that of 5-FU, which suggests that CKI also causes DNA damage (Qu et al., 2016). Thus, our *in silico* screening of RNA-seq suggested that DNA damage agents suppress PUM1-mediated mRNA decay. Notably, when variation indexes were calculated from 3,097 mRNAs bound to PUM1, instead of *bona-fide* targets of PUM1, *in silico* screening failed to detect these DNA damage agents as potential inhibitors of PUM1-mediated mRNA decay (**Figure S4**). This failure shows that the analysis of only the interaction between PUM1 and mRNAs cannot identify the stimuli that modulate PUM1-mediated gene expression control, thus highlighting the effectiveness of our approach.

Although the PUM1 targets were not always upregulated by DNA damage agents (**Figure 3E**), one important point is that the overall trend of PUM1 targets is up-regulation following DNA damage agents. Because DNA damage agents inhibit not only PUM1-mediated mRNA decay but also various signaling pathways that affect the expression of PUM1 targets, a certain set of mRNAs in PUM1 targets are not increased following DNA damage agents. Importantly, approximately ten transcripts showed up-regulation in at least two conditions and no major decrease (log2-fold-change < -1.0) in any condition. Thus, we can extract from 48 PUM1 targets 10 'core targets', of which the expression levels are tightly regulated by PUM1 under a DNA damage agent-treated condition. To further investigate the biological role of PUM1-mediated mRNA decay in DNA damage agent treated cells, the definition of core targets will provide us candidate transcripts that we should experimentally analyze in detail.

Suppression of PUM1-mediated mRNA decay by DNA damage agents.

We verified the results of the *in silico* screening by measuring the PUM1 protein level and its target mRNA levels in drug-treated cells. We selected three core targets (*PCNA*, *UBE2A*, and *ISCU* mRNAs) and one non-core target (*SLC25A12* mRNA) to analyze their expression using RT-qPCR. Corresponding to the RNA-seq data, CDDP decreased both the mRNA and protein of PUM1 (**Figure 4A and 4B**), whereas all four PUM1-target transcripts were up-regulated in HeLa TO cells (**Figure 4B**). As expected, the PUM1-target mRNAs were stabilized in CDDP-treated cells (**Figure 4C**). The inverse-correlations between PUM1 and the core targets were also identified in human colorectal carcinoma (HCT116) and human adeno carcinoma (A549) cell lines (**Figure S5A**). However, the *SLC25A12* mRNA levels did not change with CDDP in HCT116 and A549 cells. We also examined the effect of CPT on HeLa TO cells and determined that CPT decreased the PUM1 expression levels and increased only the core target mRNA levels (**Figure S5B**). These results indicated that the DNA damage agents decrease PUM1 protein levels and increase PUM1-target transcript levels. Notably, the increases of the core targets (PCNA, UBE2A, and ISCU) were common in various conditions, whereas the non-core target (SLC25A12) increase depended on the cell type, which suggests that the expression levels of the core targets were tightly regulated by PUM1-mediated mRNA decay in the cells.

To investigate whether a cause-and-effect relationship exists between the PUM1 decrease and PUM1-target increase, we prepared cell lines that over-expressed PUM1 or PUM1 mutant that lacked the RNA-binding domain (Δ PUM-HD) (**Figure 5A**). In these over-expressed cell lines, PUM1 or Δ PUM-HD existed even after the addition of CDDP (**Figure 5B**). We analyzed the mRNA expression levels of the PUM1 targets in PUM1 over-expressed cells (**Figure 5C**). CDDP did not significantly increase the expression of *PCNA* and *SLC25A12* in the PUM1 over-expressed cells. *UBE2A* and *ISCU* showed slight increases; however, the extents of these increases were significantly lower than those identified in non-treated cells. In contrast, the PUM1 targets were significantly increased in the cells that over-expressed Δ PUM-HD after CDDP treatment, that is, nearly the same extent as the control cells. These results demonstrated that the loss of PUM1 activity is responsible for the up-regulation of PUM1 targets under DNA damage.

Resistance of cells to DNA damage agents by suppressing PUM1-mediated mRNA decay.

DNA damage induces cellular apoptosis (Roos and Kaina, 2006, 2013) and the core targets of PUM1 (PCNA, UBE2A, and ISCU) are involved in the DNA damage response (Moldovan et al., 2007; Somasagara et al., 2017; Tong and Rouault, 2006); thus,

we hypothesized that cells acquire resistance to DNA damage agents by suppressing PUM1-mediated mRNA decay. To test this hypothesis, we quantified the viability of cells that over-expressed wild or mutant PUM1 after CDDP treatment. The survival rate of the PUM1 over-expressed cells was 49%, which was significantly lower than that of the control cells (**Figure 5D**). In contrast, the overexpression of Δ PUM-HD, which did not restore the PUM-mediated mRNA decay, did not reduce the survival rate (**Figure 5D**). Taken together, our results suggest that the loss of PUM1 in response to DNA damage agents provides cells with resistibility to the drugs through the increment of PUM-target mRNAs (**Figure 5E**).

Generality of *in silico* screening: application to UPF1 study.

To demonstrate the generality of our *in silico* screening, we applied our approach to up-frameshift protein 1 (UPF1). UPF1 is a well-known core factor of the nonsense-mediated mRNA decay (NMD) to eliminate aberrant mRNAs containing premature termination codon (PTC) that have a potential to produce harmful proteins (Imamachi et al., 2012; Isken and Maquat, 2007; Maquat, 2004; Schweingruber et al., 2013); however, many normal mRNAs are also regulated by UPF1 through RNA degradation (Nasif et al., 2018). Here, we focused on the 51 UPF1 targets, which were both stabilized and up-regulated by UPF1 depletion (Imamachi et al., 2016). To perform *in silico* screening, we calculated the log2-fold change of UPF1 and the variation indexes of UPF1 targets and analyzed the correlation between the variation index and fold change of UPF1 (**Figure 6A**).

The *in silico* screening of RNA-seq data suggested that Zaire ebolavirus (EBOV) and Reston ebolavirus (RESTV) suppress UPF1-mediated mRNA decay, whereas rapamycin promotes UPF1-mediated mRNA decay (**Figure 6A**). A previous study demonstrated that rapamycin down-regulated UPF1-regulated mRNAs, which was consistent with our screening result (Martinez-Nunez et al., 2017). Moreover, we verified the result of the *in silico* screening experimentally. HEK293 cells treated with rapamycin showed an increase in the UPF1 protein level and decreases in UPF1 targets, such as *CYP2S1* and *DDIT3* (**Figure 6B and 6C**). These results indicated that rapamycin causes an inverse-correlated effect on UPF1 and its targets, thus demonstrating that our *in silico* screening of RNA-seq data is applicable to the other RBP study.

Discussion.

We present a combinatorial analysis that combines RNA-seq techniques to identify *bona-fide* targets of the RBP of interest and a novel computational framework to identify the stimuli that modulate RBP-mediated mRNA decay. We employed this analysis to dissect PUM1 and determined that the downregulation of PUM1 by DNA damage agents leads to an up-regulation of a subset of PUM1-target mRNAs, including mRNAs that encode DNA damage response (DDR) proteins. In addition, PUM1 down-regulation enhanced cell viability under DNA damage agents. Thus, we identified a novel biological function of PUM1 in DDR. It is worth noting that the stabilization of transcripts in DNA damage is a reasonable response of cells; transcripts produced from damaged DNA tend to produce abnormal proteins. To obtain sufficient amounts of undamaged transcripts for survival, RNA stabilization that utilizes existing mRNAs is an expedient mechanism in DDR.

Our *in silico* screening is based on the analysis of the functional relationship between PUM1 and *bona-fide* targets of PUM1. By analyzing the alterations of the mRNA expression levels of both PUM1 and its targets in various conditions *in silico*, we could successfully identify the previously unknown function of PUM1.We emphasize that the *in silico* screening should be performed with functional targets of PUM1, rather than transcripts only bound to PUM1. When the mRNAs bound to PUM1 were applied for *in silico* screening, we failed to determine DNA damage reagents as regulators of PUM1-mediated mRNA decay (**Figure S4**). This failure indicates that binding of PUM1 to a transcript is only a necessary condition for PUM1 to exhibit a function on the transcripts. Although current studies mainly focus on identifying transcripts bound to the RBPs of interest using RIP-seq or CLIP-seq (Dominguez et al., 2018; Lambert et al., 2014; Nostrand et al., 2016; Sundararaman et al., 2016; Wheeler et al., 2018), our study highlights the importance of identifying *bona-fide* targets of the particular RBP in analysis of their biochemical functions.

Our combinatorial analysis indicated a distinct function of PUM1 from other studies. The biological functions of PUM1 and its homologous proteins have been extensively analyzed in various organisms (Morris et al., 2008; Wang et al., 2018; Wickens et al., 2002). In lower eukaryotes, such as *S. cerevisiae*, Puf proteins inhibit cell differentiation and regulate organelle biogenesis (Gerber et al., 2004). In higher eukaryotes, such as *C. elegans*, *D. melanogaster*, and *Xenopus*, PUM proteins regulate several developmental processes, including embryogenesis, gametogenesis/gamete maturation (Quenault et al., 2011), and neuronal development (Kaye et al., 2009). In mammalian cells, PUM proteins are suggested to be involved in the transition from the

quiescent to growth phase (Kedde et al., 2010) and spermatogenesis (Chen et al., 2012). Although these features of PUM were not elicited from the GO term analysis of PUM1-target mRNA in this study, we determined that PUM1-bound mRNAs were associated with the components related to development and cell differentiation by PANTHER pathway analysis (**Table S2**). Importantly, the majority of PUM1-bound mRNAs were not degraded by PUM1 in HeLa TO cells under normal conditions. The functional difference of the biological role between PUM-bound mRNAs and PUM1-mediated mRNA decay targets suggests that binding information only provides the potential function of PUM. However, it does not provide the actual function of PUM in a specific cell condition. This gap between binding and function prompts further questions, such as why and how some mRNAs are selected by PUM1 as degradation targets, whereas other mRNAs are only bound to PUM1. One possibility is that PUM1 regulates the translation and/or localization of specific mRNAs rather than their stability. Puf3, a yeast homologue of the PUM gene, contributes to the mitochondrial localization of a certain set of mRNAs (García-Rodríguez et al., 2007). Moreover, mammalian Pum2 might be involved in local translation in neurons (Vessey et al., 2006, 2010). One potential answer to the question of how to select specific RNAs for degradation is that mRNAs may be co-regulated with multiple RBPs, the concept introduced as RNA regulon (Keene, 2007). For the mRNAs incorporated in RNA regulon, the effect of PUM1 depletion may be minimized because other RBPs degrade the mRNAs (compensation). Although additional studies are required, these considerations suggest the necessity of analyzing the networks of RBPs and their functional target RNAs with RBPome (RNA-Binding Proteome) levels to understand the complete picture of RBPs' functions.

We showed that core targets of PUM1, such as mRNAs encoding PCNA, UBE2A, and ISCU, have a role in DNA repair (Giglia-Mari et al., 2011; Lord and Ashworth, 2012). For example, damaged DNA is repaired by DNA helicase, XPD, which includes an iron-sulfur (Fe-S) cluster (Rudolf et al., 2006). As ISCU regulates the generation of Fe-S clusters (Tong and Rouault, 2006), an increase of ISCU is thought to enhance the DNA repair activity by activating XPD (Favaro et al., 2010). Moreover, PCNA is ubiquitinated and is involved in the UBE2A-dependent DNA repair pathway in response to DNA damage caused by chemical reagents, such as anticancer drugs (Hoege et al., 2002; Somasagara et al., 2017; Zhang and Yu, 2012). Considering their role in cancer, PCNA and UBE2A are thought to be therapeutic targets because the down-regulation of these two genes reduces DNA damage tolerance, decreasing the survival of cancer cells (Sanders et al., 2017; Stoimenov and Helleday, 2009; Wang, 2014). Cancer cells frequently develop resistance to chemical therapies, a phenomenon referred to as

drug resistance (Housman et al., 2014). The inhibition of drug resistance used in conjunction with traditional therapy will sensitize cancer cells to the drug and thus increase the efficacy of chemotherapy. To inhibit drug resistance, researchers are currently focusing on the defection of DDR in cancer cells (Curtin, 2012; O'Connor, 2015; Pearl et al., 2015). Up-regulated DNA repair pathways will cause resistance to DNA-damage causing drugs, such as CDDP. Thus, inhibitors of DDR have the potential to sensitize cancer cells to the anti-cancer drugs. However, combinations of DDR inhibitors with traditional therapies have been less successful. Our results demonstrated that constitutive expression of PUM1 after CDDP treatment inhibits the increase of PUM1 targets, leading to susceptibility for CDDP. This study may present alternative insights to reduce the drug resistance of cancer cells.

Despite the previously described successes, our method fails to identify previously known PUM1-mediated mRNA decay targets. This failure may be a result of the definition of PUM1 targets. In this study, we defined a PUM1 target as an mRNA that is bound to PUM1 and is stabilized in PUM1 KD HeLa TO cells. This definition will exclude condition-specific PUM1 targets. For example, post-translational modified PUM1 may degrade a certain set of mRNAs (Arif et al., 2009; Mukhopadhyay et al., 2008). Phosphorylated PUM1 in growth-factor stimulated cells are known to degrade *p27* mRNA, which is not listed in our *bona-fide* targets of PUM1 (Kedde et al., 2010). To understand PUM1 function more generally, it is necessary to include post-translational modification in our analytical pipeline, although technically challenging. Moreover, PUM1 effects related to differentiation and mitosis should be cell-type specific or condition-specific and thus negligible in HeLa TO cells. If we re-define PUM1-mediated mRNA decay in each cell-cycle phase or in stem cells, novel features of PUM1 may be identified by our methodology.

The capability of *in silico* screening depends on the number and variety of RNA-seq deposited in publicly available databases. Currently, our database includes 187 conditions (**Table S3**). These conditions are only a small fraction of biological stimuli, considering that more than 5,000 inhibitors for cell biology are commercially available. Although the current variation in our framework is limited, we expect to have a rich RNA-seq dataset for *in silico* screening within several years because of the dramatic increase of RNA-seq data in recent years. Moreover, we can expand the biological conditions for *in silico* screening by applying microarray data. In GEO, there are approximately 1,400 series of array data when searching with the keywords 'inhibitor' and 'human', whereas only 400 RNA-seq data exist in the same condition.

In conclusion, our method provides a genome-wide view of RBP-mediated

mRNA decay and its regulation, thus providing biological hypotheses for the further investigation of RBP functions. As more diverse gene expression datasets become available, we believe there is potential for our methodology to be a standard strategy for understanding the biological functions of RBPs.

Acknowledgments

We would like to thank our lab members for the fruitful discussions and help with the experiments. This work was supported by grants from MEXT KAKENHI (15H04642, 16H06279). T.Y. received the JSPS Research Fellowship for Young Scientists and is supported by a Grant-in-Aid for JSPS Fellows (17J11266).

Author contributions

Conceptualization, T.Y. and N.A.; Methodology, T.Y., N.I., and K.I.; Software, T.Y. and N.I.; Formal Analysis, T.Y. and N.I.; Investigation, T.Y. and T.K.; Resources, T.K. and M.N.; Data Curation, T.Y. and N.I.; Writing – Original Draft, T.Y.; Review & Editing N.I., K.I., T.K., M.N., and N.A.; Supervision, N.A.

Declaration of Interests

The authors declare there are no competing interests.

Methods

Contact for Reagent and Resource Sharing

Further information and requests for resources and reagents should be directed to and will be fulfilled by the Lead Contact, Nobuyoshi Akimitsu (akimitsu@ric.u-tokyo.ac.jp).

Experimental Model and Subject Details

Cell Culture and Cell Lines

HeLa Tet-off cells (HeLa TO cells) (Clontech, Palp Alto, CA) and A549 cells (kindly provided by Dr. Nobukuni) were grown in Dulbecco's modified Eagle's medium (DMEM) (Wako, Osaka, Japan) supplemented with 10% heat-inactivated fetal bovine serum (FBS) (Life Technologies, Grand Island, NY) at 37 °C in a humidified incubator (Thermo Fisher Scientific, Walthman, MA) with 5% CO_2. HCT116 (obtained from ATCC) cells were maintained in McCoy's 5A medium (Life Technologies) with 10% FBS (Life Technologies) at 37 °C with 5% CO_2. All cell lines were banked directly after being purchased from vendors and were used at low passage numbers (less than twenty).

Method Details

Plasmid construction

FLAG-PUM1, FLAG-PUM2, and FLAG-ΔPUM-HD were built using conventional restriction enzyme cloning.

PUM1 and PUM2 cDNA were amplified from a cDNA library. In brief, a first strand cDNA library was synthesized using total RNA isolated from HeLa Tet-off cells and SuperScript II Reverse Transcriptase (Thermo Fisher Scientific). PCR amplification was performed using the following primer sets:

For PUM1

Forward: 5'-ccgGATATCagcgttgcatgtgtcttgaag-3' (Capital letters represent an EcoRV site)

Reverse: 5'-ccccccctaatggtatcatctgaGCGGCCGCataagaat-3' (Capital letters represent a NotI site)

For PUM2

Forward: 5'-tgaGAATTCtaatcatgattttcaagctcttgc-3' (Capital letters represent an EcoRI site)

Reverse: 5'-tgaCTCGAGttacagcattccatttggt-3' (Capital letters represent an XhoI site)

The PCR product was digested with the corresponding enzymes and inserted into the digested pcDNA 3.1 Hygro vector with a FLAG tag sequence (5'-

ACTAGTCCAGTGTGGTGGAATTCTGCA-3') between BamHI and EcoRV.

To construct the PUM1 mutant, which lacks the RNA-binding domain (ΔPUM-HD), the PUM1 mutant region was amplified from FLAG-PUM1 with the following primer sets:

Forward: 5'-aaaGATATCagcgttgcatgtgtcttg-3' (Capital letters represent an EcoRV site)

Reverse: 5'-attcttatgGCGGCCGCtcactgctcctgccagaagg-3' (Capital letters represent a NotI site)

The PCR product was digested with the corresponding enzymes and inserted into the digested pcDNA 3.1 Hygro vector with the FLAG tag sequence.

All plasmids were prepared using the PureYield Plasmid Midiprep System (Promega, Madison, WI) for transfection to cells.

Transfection

The plasmids were transfected into HeLa TO cells using Lipofectamine 2000 (Thermo Fisher Scientific) according to the manufacturer's protocol. In brief, the day prior to the transfection, the cells were plated into 12 wells (for RIP-seq and BRIC-seq, 10 cm dish) with 1.5×10^5 cells/mL density. For each well, 2 μL of Lipofectamine 2000 reagent mixed with 500 μL of OptiMEM medium (Life Technologies) were added to the 1.0 μg plasmid. After 20 minutes of incubation at room temperature, the mixture was added to the cells, followed by a 6-hour incubation at 37 °C with 5% CO_2. The OptiMEM medium was subsequently replaced by culturing medium (DMEM with FBS). Transfected cells were used for further studies at 24-hours post-transfection.

All siRNAs were synthesized by Hokkaido System Science (Hokkaido, Japan). siRNAs were transfected into cells using Lipofectamine RNAi MAX (Thermo Fisher Scientific), according to the manufacturer's protocol. Briefly, siRNA duplexes (final concentration, 10 nM) were transfected into cells, followed by incubation for 6-hours in 37 °C / 5% CO_2, and the medium was subsequently changed. The cells were then incubated for 48-hours. The siRNA sequences are listed in **Table S4**.

Sample preparation for RNA-immunoprecipitation sequencing (RIP-seq)

Plasmid cloned FLAG-tagged PUM1 or PUM2 was transfected into HeLa TO cells (1.5×10^6 in 10 cm dish) using Lipofectamine 2000 (Thermo Fisher Scientific), as described in the previous section. After 24-hours, the cells were harvested and washed in cold PBS. The cell pellets were lysis by the addition of 300 μL of polysome lysis buffer (PLB: 100 mM KCl, 5 mM $MgCl_2$, 10 mM Hepes, pH 7.0, 0.5% NP-40, Recombinant RNase inhibitor (Takara) and protease inhibitor cocktail (Sigma-Aldrich)). The lysate was

subsequently sonicated for 2 min with 15 second intervals using a Bioruptor UCD-250 (Cosmo Bio, Tokyo, Japan). After 15 min of centrifugation at 12,000 rpm, 10 μL of supernatants were used for the input protein sample, 30 μL of supernatants were used for the input RNA sample, and the remaining were used for immunoprecipitation (IP).

Antibody-bead conjugates were prepared as follows: One hundred μL of protein G Dyna beads (Thermo Fisher Scientific) were washed three times in PLB and were resuspended in 1 mL of PLB. Fifteen μL of anti-FLAG M2 mouse monoclonal antibody (SIGMA) were added to the beads. After rotating the mixture at 4 °C overnight, the beads were washed with 1 mL PLB two times.

The supernatants were mixed with antibody-bead conjugates and rotated for 2-hours at 4 °C. The beads were washed six times in ice-cold NT2 buffer (50 mM Tris, pH 7.4, 150 mM NaCl, 1 mM $MgCl_2$, 0.05% NP-40). After the final wash, the beads were resuspended in 1 mL of NT2 buffer. In 1 mL lysate, 40 μL of lysate were used for the protein sample and the remaining was used for the RNA sample.

For RNA isolation, 200 μL of 100 mM Tris/50 mM NaCl and 600 μL of ISOGEN LS (Nippon Gene, Tokyo, Japan) were subsequently added, followed by RNA isolation according to the manufacturer's protocol. Prior to sequencing, the isolated RNA was quantified by RT-qPCR, and the size distribution was assessed using an Agilent 2100 Bioanalyzer. The isolated RNA was used for high-throughput sequencing. A RIP-seq complementary DNA library was prepared from 1 μg of total RNA using the TruSeq RNA Library Prep Kit v2 (Illumina, San Diego, CA), according to the manufacturer's protocol. Thirty-six base pair single-end read RNA-seq tags were generated using an Illumina HiSeq 2500, according to the standard protocol. The fluorescent images were processed to nucleotide sequences using the analysis Pipeline supplied by Illumina.

Motif identification

To validate the putative binding motif for PUM in the 3'UTRs of the transcripts bound to PUM, we performed *de novo* motif discovery on the sequences using multiple EM for motif elicitation (MEME). To reduce the calculation time, the top 100 transcripts of the RIP-seq fold change were selected for the MEME analysis. Here, 3'UTR was defined in the RefSeq annotation data.

Bromo-uridine (BrU) immunoprecipitation chase-deep sequencing (BRIC-seq)

BRIC was performed as previously described (Yamada et al., 2018). In brief, cells were incubated at 37 °C in the presence of 150 μM bromo-uridine (BrU) (Wako Chemical, Tokyo, Japan) for 24-hours in a humidified incubator with 5% CO_2. Cells were harvested

at the indicated time points after replacing BrU-containing medium with BrU-free medium. Total RNA was isolated using RNAiso Plus (Takara), followed by the isolation of BrU-labeled RNA using anti-BrdU mouse antibody (clone 2B1, MBL, Nagoya, Japan). The isolated RNA was used for high-throughput sequencing as described in the "Sample preparation for RNA-immunoprecipitation sequencing (RIP-seq)" section.

Sample preparation of IP-Mass spectrometry analysis

The preparation of cell lysate for IP-mass is exactly the same procedure for RIP-seq (refer to the first paragraph of the "Sample preparation for RNA-immunoprecipitation sequencing (RIP-seq)" section). To elute proteins with little antibody contamination, we cross-linked the antibody to the beads. One hundred μL of Dynal protein G beads (Thermo Fisher Scientific) were washed three times in PLB and were resuspended in 1 mL of PLB. Fifteen μL of anti-FLAG M2 mouse monoclonal antibody were added to the beads. After rotating the mixture at 4 °C overnight, the beads were washed two times with 1 mL of 100 mM sodium borate, pH 9.0. The beads were re-suspended with 1 mL DMP/borate solution and were incubated for 15 minutes at room temperature. After the removal of the buffer, the beads were re-suspended with 1 mL fresh DMP/borate solution and were incubated for 30 minutes at room temperature. The beads were subsequently washed two times with 1 mL of 50 mM Glycine, pH 2.5. Finally, the beads were washed two times with PLB and were stored with PLB.

Prior to mixing the beads and cell lysate, cells were treated with 3 μL of RNase A + T1 mixture (1 μg/μL RNaseA and 40 U/μL RNaseT1) for 10 minutes on ice. The cell lysates were mixed with antibody-bead conjugates and rotated for 2-hours at 4 °C. The beads were washed six times in ice-cold NT2 buffer. After the final wash, the beads were resuspended in 20 μL of 0.02% RapiGest to elute the proteins. The beads in RapiGest solution were vortex and were incubated for 30 minutes at 67 °C. After spin down of the beads, the supernatants were used for mass spectrometry.

Liquid Chromatography-Tandem Mass Spectrometry (LC/MS/MS)

A capillary reverse phase HPLC-MS/MS system (ZAPLOUS System; AMR Inc.), composed of a Paradigm MS4 quadra solvent delivery device (Michrom BioResources), an HTC PAL autosampler (CTC Analytics), and a Finnigan LTQ orbitrap XL mass spectrometer (Thermo Scientific) equipped with an XYZ nanoelectrospray ionization source (AMR Inc.), was used for the LC/MS/MS analysis. Aliquots of trypsinized samples were automatically injected onto a peptide CapTrap cartridge (2.0 × 0.5 mm inner diameter, Michrom BioResources) attached to an injector valve for desalting and

concentrating the peptides. After washing the trap with 98% H_2O, 2% AcCN, and 0.2% TFA, the peptides were loaded into a separation capillary reverse phase column (Monocap C18 150 × 0.2 mm inner diameter, GL-Science) by switching the valve. The eluents used were as follows: A, 98% H2O, 2% AcCN, 0.1% HCOOH; and B, 10% H_2O, 90% AcCN, 0.1% HCOOH. The column was developed at a flow rate of 1.0 μL/min, with a concentration gradient of AcCN: from 5% B to 35% B for 100 min, followed by 35% B to 95% B for one minute, maintained in 95% B for nine minutes, from 95% B to 5% B for one minute, and finally re-equilibrating with 5% B for nine minutes. Effluents were introduced into the mass spectrometer via the nanoelectrospray ion interface that held the separation column outlet directly connected with a nanoelectrospray ionization needle (PicoTip FS360–50-30; New Objective Inc.). The ESI voltage was 2.0 kV, and the transfer capillary of the LTQ inlet was heated to 200 °C. No sheath or auxiliary gas was used. The mass spectrometer was operated in a data-dependent acquisition mode, in which the MS acquisition with a mass range of m/z 420–1600 was automatically switched to MS/MS acquisition under the automated control of Xcalibur software. The top 4 precursor ions were selected by an MS scan, with Orbitrap at a resolution of r = 60000, and for the subsequent MS/MS scans by an ion trap in the normal/centroid mode, using the automated gain control (AGC) mode with AGC values of 5.00 × 105 and 1.00 × 104 for full MS and MS/MS, respectively. We also employed a dynamic exclusion capability that enabled the sequential acquisition of the MS/MS of abundant ions in the order of their intensities with an exclusion duration of two minutes and exclusion mass widths of −5 and +5 ppm. The trapping time was 100 milliseconds with the auto gain control on.

Reverse transcription-quantitative real-time polymerase chain reaction (RT-qPCR)

The isolated RNA was reverse transcribed into cDNA using the PrimeScript RT Master Mix (Takara). cDNA was amplified using the primer sets listed in **Table S4** with SYBR Premix Ex Taq II (Takara) in accordance with the manufacturer's instructions. RT-qPCR analysis was performed using a Thermal Cycler Dice Real Time System (Takara). The GAPDH and PGK1 mRNAs were used for transcript normalization. For the UPF1 study, SDHA mRNA was used for normalization. The relative value of the transcript was calculated using the comparative CT method (ΔΔCT). We analyzed three biological replicates with two technological replicates for each experiment.

Western blotting

Total protein extracts were prepared in RIPA buffer and separated on a 10% sodium

dodecyl sulfate polyacrylamide gel. The proteins were transferred onto a polyvinylidene fluoride membrane (Millipore). The membrane was blocked with 3% BSA/Tris-buffered saline that contained 0.1% Triton X-100 (TBST) and was incubated with a 1:500 dilution of anti-PUM1 rabbit polyclonal antibody (Sigma-Aldrich, #HPA027424), 1:250 dilution of anti-PUM2 rabbit monoclonal antibody (Abcam, #ab92390), 1:1000 dilution of anti-GAPDH mouse monoclonal antibody (MERK, #MAB374), 1:4000 dilution of anti-FLAG M2 mouse monoclonal antibody (Sigma-Aldrich, #F1804), or 1:1000 dilution of anti-CNOT1 rabbit polyclonal antibody (Protein Technology, #14276-1-AP) for 1 hour at room temperature. All antibodies were diluted using IMMUNO SHOT reagent1 (COSMO BIO, Tokyo, Japan). After three washes of the membrane with TBST, the membrane was incubated with a 1:10000 or 1:5000 dilution of horseradish peroxidase (HRP)-linked secondary antibodies in IMMUNO SHOT reagent2 (COSMO BIO) for one-hour at room temperature. The proteins were visualized using Immobilon western chemiluminescent HRP substrate (MERK), according to the manufacturer's instructions.

Actinomycin D chase assay

For RNA stability measurements, HeLa TO cells were treated with 1 μg/mL actinomycin D (dissolved in DMSO [Sigma-Aldrich]). After 30 minutes of incubation, the cells were harvested at the indicated time points, and RNA isolation, cDNA synthesis, and RT-qPCR were performed as previously described.

Assays for cell proliferation with CDDP treated cells

The proliferation of the HeLa TO cell lines was measured using the Cell Counting kit-8 (Dojindo, Kumamoto, Japan). HeLa TO cells were subcultured in 96-wells with 1.5×10^5 cells/mL density. The next day, the cells were transfected with empty vector, FLAG-PUM1, or FLAG-ΔPUM-HD, as described in the transfection section. After 24 hours of incubation, 0.5 mg/mL of CDDP was added to the cells for seven hours. Then, 10 μL of Cell Counting Kit-8 in 100 μL of culturing medium were added, and the cells were incubated for 30-minutes. The absorbance of 595 nm in each well was measured using Infinite F200 (TECAN, Switzerland). The mean absorption of five independent wells was calculated with the s.e.m. for each biological condition. The cell viability was defined by the absorbance of cells with CDDP normalized by that without CDDP.

Quantification and Statistical Analysis

Preprocessing, mapping, and quantification of sequencing data

Low quality reads were discarded using the FASTX-toolkit and reads that contained less

than 10 bp were eliminated using Bowtie (Langmead et al. 2009). The filtered reads were mapped to the reference human genome (hg19) and transcriptome from RefSeq downloaded from illumine iGenomes using TopHat (version 2.0.12) (Kim et al. 2013). The mapped reads were quantified to measure the RNA expression level for each gene using Cufflinks (version 2.1.1) (Trapnell et al. 2010). The abundance of RefSeq transcripts was calculated from the BRIC-seq and RIP-seq sequence reads, based on the reads per kilobase of exon model per million mapped reads (RPKM), as a means of normalizing for the gene length and depth of sequencing. Transcripts with RPKM≧ 1 were considered expressed for subsequent analysis.

Identification of transcripts bound to PUM

We set the threshold of the fold discovery rate, calculated using Cufflinks (version 2.1.1), to less than 0.05 for the transcripts of which the RPKM is greater than 1.0 in the corresponding RIP-PUM sample.

Calculation of RNA half-life and estimation of significant fold-change with PUM KD

The RNA-half life was calculated as previously described. Briefly, the relative expression data of each transcript at each time point were normalized using the 97.5% percentile. To predict an RNA decay curve, the normalized expression data were fitted to the first order exponential RNA decay model. The RNA half-life and its variance are estimated from the fitting curve and time points. In this study, the RNA half-lives were determined for 12,496 mRNAs in control cells.

To determine the significant change of the RNA half-lives, the distributions of the RNA half-lives between two conditions were compared using Welch's *t*-test. Here, the criteria for significant stabilization were (1) log2-fold change of half-life > 1 (for de-stabilization, < 0.5) in PUM KD cells and (2) p-value < 0.05 (Welch's *t*-test).

Database search and label-free semiquantitative proteomic analysis

MS/MS data were processed with Mascot software (version 2.5.1, Matrix Science) against the SwissProt_2016_07 database at a fragment tolerance of 0.6 Da and a parent tolerance of 5.0 ppm, considering the fixed peptide modification by carbamidomethyl (C), variable peptide modifications by methionine oxidation, and phosphorylation, including phosphoserine, phosphothreonine, and phosphotyrosine. The analysis of the data was conducted with Scaffold software (version 4.5.3, Proteome Software). The label-free semiquantitative values were determined using Expressionist Refiner MS software (GeneData). After pre-processing (noise subtraction, RT alignment, and peak detection)

and importing the identification results from Mascot software, the relative ion intensities were calculated and normalized via the Lowess normalization method. The thresholds of the peptides were set to 95% minimum and the thresholds of the proteins were set to 99% minimum with 3 peptides minimum.
To determine the PUM-associated proteins, we set the threshold to a five-fold enrichment in PUM immunoprecipitants compared to the control.

Statistical overrepresentation test

Protein Analysis THrough Evolutionary Relationships (PANTHER) analysis was performed with 2,671 mRNAs at http://pantherdb.org/. The reference mRNA list was defined as 10,907 HeLa expressing mRNAs of which the expression is greater than 1 RPKM in RNA-seq.

Motif searches

The 3'UTRs of the sequences were retrieved from GenBank (RefSeq, hg19). The PUM motif was searched using MEME (http://meme-suite.org/). To assign statistical significance to the reported PUM motif, we applied the *E*-value, which is automatically calculated in the MEME program.

In silico screening of RNA-seq

To generate the complete datasets for screening, GEO was queried in terms of 'human', 'inhibitor', or 'stress'. After the collection of the SRA files, mapping and quantification of the RNA-seq data were performed as described in the "Preprocessing, mapping, and quantification of sequencing data" section. For each RNA-seq data, the log2-fold-changes of the PUM1 and PUM1 targets were calculated. To estimate the correlation between the PUM1 and PUM1 targets, the "Variation Index of targets" was calculated as follows, *Variation Index* = "the number of increased PUM1 targets (log2-fold-change > 1)" - "the number of decreased PUM1 targets (log2-fold-change < -1)". A scatter plot was used to investigate the potential relationship between the log2-fold-change of PUM1 and the Variation index. In the scatter plot, RNA-seq that suggests a stimulus inhibits PUM1-mediated mRNA decay will be plotted in the second quadrant, whereas RNA-seq that suggests a stimulus promotes PUM1-mediated mRNA decay will be plotted in the fourth quadrant. All codes are freely available at the github repository (https://github.com/Imamachi-n/AutoNGS).

For *in silico* screening with the UPF1 and UPF1 targets, we focused on 51 mRNAs that are stabilized and up-regulated in UPF1 KD cells. We identified many

transcription factors in the UPF1 target, of which the expression levels are regulated in a complex manner. The complicated regulation of gene expression may interrupt the increase in UPF1 targets when the targets were stabilized by the decrease in UPF1. As our *in silico* screening relies on the simple assumption that the amounts of transcripts increase by the stabilization of transcripts, the collapse of the assumption in the *in silico* screening will significantly decrease the accuracy of the screening. To systematically avoid this failure, we also considered the increase of mRNA amounts by UPF1 KD.

Statistical test in q-PCR

The fold expression was calculated as $2^{-\Delta\Delta CT}$. Statistical significance was defined as a p-adjusted < 0.05. For bar plots, error bars represent 1 standard deviation and asterisks (*) indicate statistically significant changes.

Data and Software Availability

Software

Shell scripts, python codes, and R scripts for the RNA half-life calculation are freely available at the github repository (https://github.411com/AkimitsuLab/scripts_for_BRIC-seq_data_analaysis). There are two folders named "half-life_calculation" and "half-life_calculation_for_DEG_analysis" to calculate the RNA half-life and identify the significant change of RNA half-lives between two conditions, respectively. Codes for *in silico* screening are available at https://github.com/Imamachi-n/AutoNGS. For drawing scatter plots and a heatmap, Jupyter notebooks are available at https://github.com/ToshimichiYamada/PUM_study.

Data

The accession numbers for the mass spectrometry data reported in this paper are ProteomeXchange: PXD009849 (http://www.proteomexchange.org/) or JPOST: JPST000424 (https://repository.jpostdb.org/).

1 **Figure Legends**

Figure 1

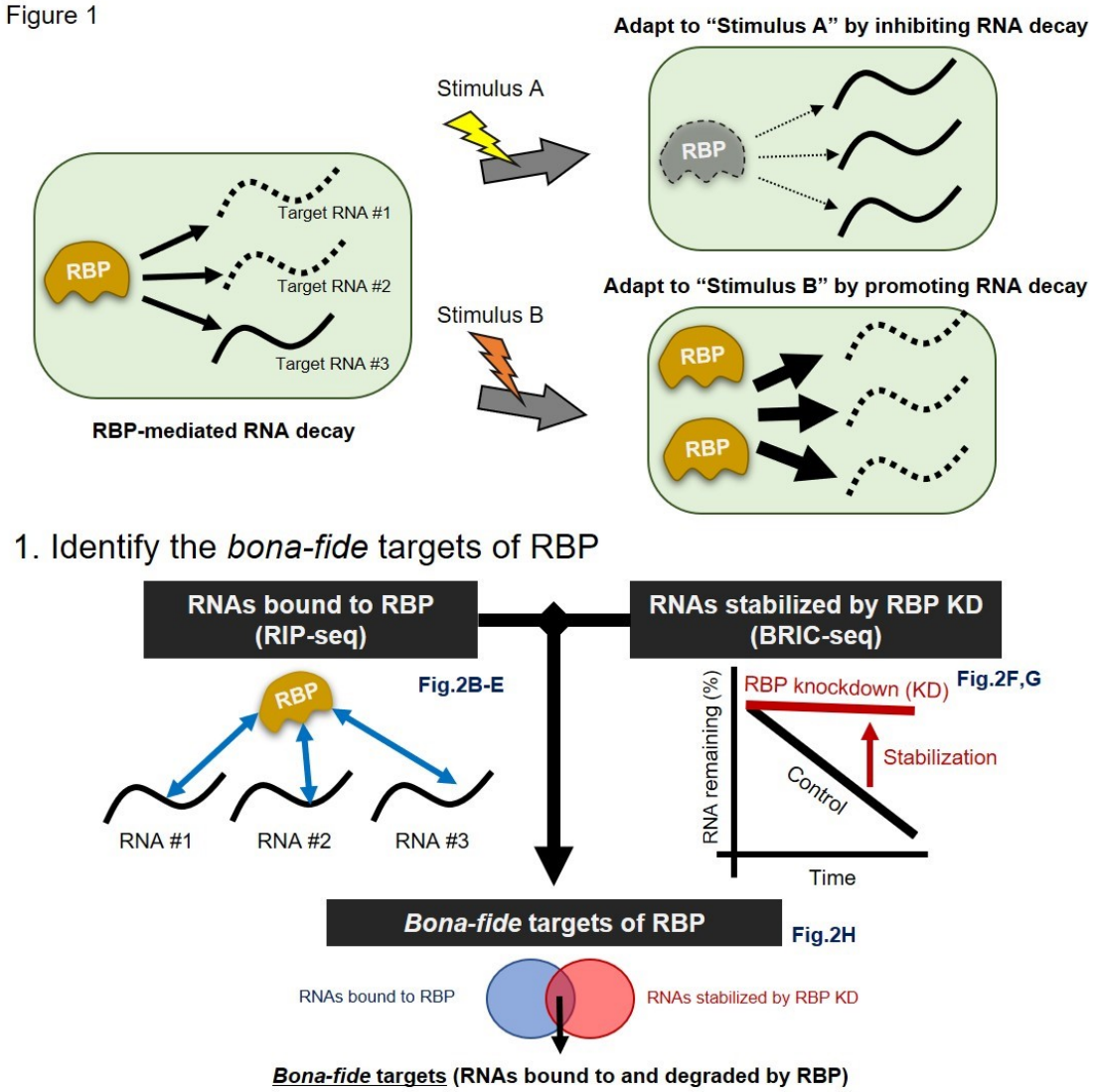

2

Figure 1. Schematic strategy to analyze the biological role of RBP-mediated mRNA decay RBP, RNA binding protein. RIP-seq, RNA immunoprecipitation sequencing. BRIC-seq, 5'-bromo-uridine (BrU) immunoprecipitation chase-deep sequencing analysis.

Figure 2

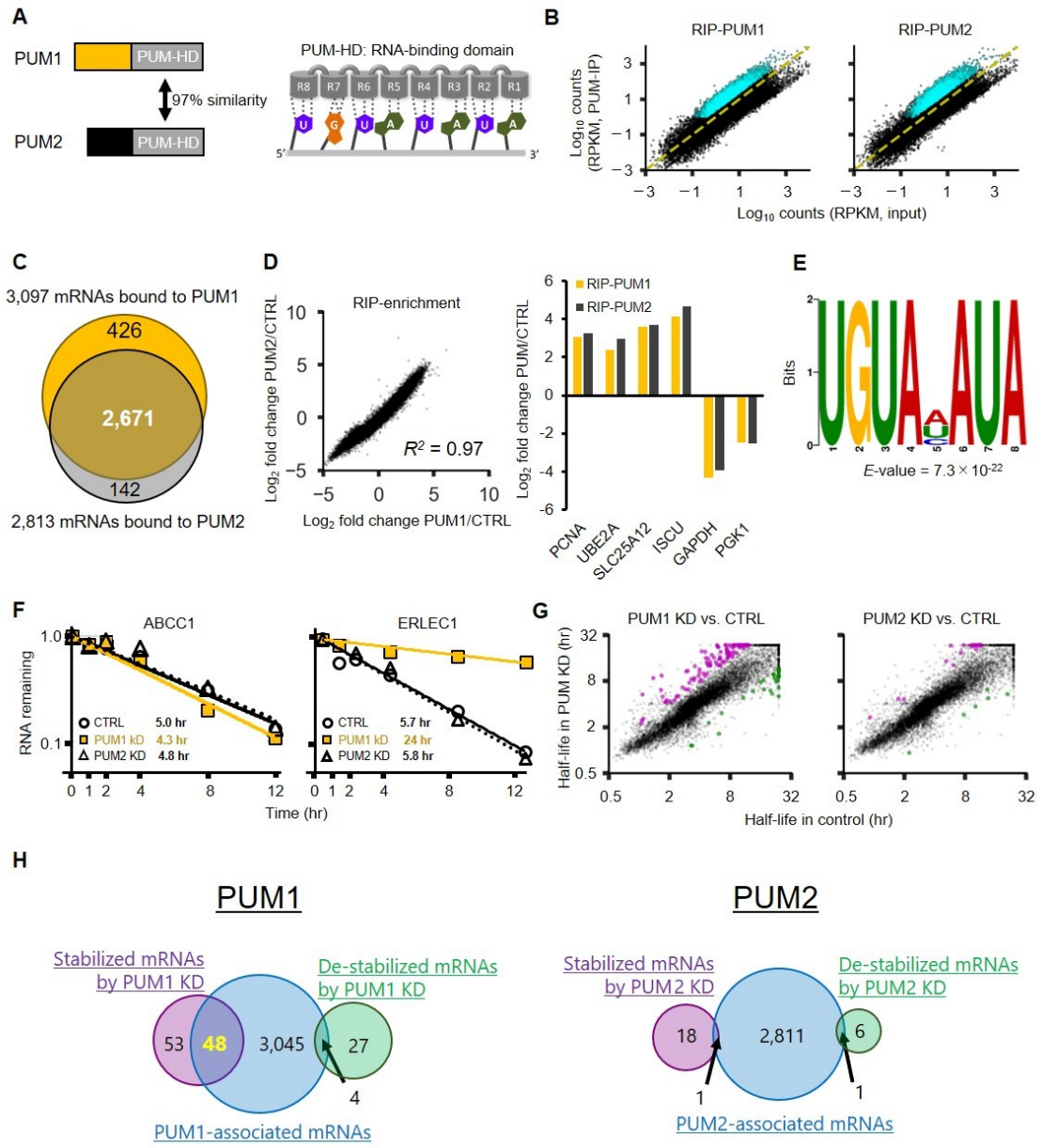

Figure 2. Identification of target mRNAs. (A) Schematics of human PUM1 and PUM2 proteins. Both PUM proteins share the RNA-binding domain (PUM-HD) with a high similarity at the C-terminal. PUM-HD comprises eight repeats, named R1 to R8, which bind to a specific RNA base. (B) Scatter plots of RIP-seq data of PUM1 (left) and PUM2 (right) showing the RPKM for each transcript identified in the RIP-seq data (RIP-PUM) against the RPKM for the same transcript in the input sample. Cyan indicates PUM-binding transcripts (FDR < 0.05). (C) Venn diagram showing overlap between PUM1-binding mRNAs and PUM2-binding mRNAs. (D) A scatter plot showing the correlation

of fold enrichment levels of RIP-PUM1-seq against RIP-PUM2-seq (left). Bar graphs display representative data of RIP-seq (right). (E) *De novo* sequence motif enriched above background with associated *E*-value. (F) Representative decay plots of mRNA (left: *ABCC1*, right: *ERLEC1*) determined by BRIC-seq. mRNA decay was calculated with the cells treated with siRNA targeting control (circle, black), PUM1 (square, yellow), or PUM2 (triangle, black). In each decay plot, data were curve fitted with an exponential function (solid and dashed lines). (G) Scatter plots show the mRNA half-life for each transcript calculated by BRIC-seq of PUM1 KD cells (left) or PUM2 KD cells (right) against the half-life for the same transcript in the control cells. Significantly stabilized transcripts are shown in magenta spots, whereas significantly de-stabilized transcripts are shown in green spots. (H) Venn diagram illustrating the overlap of the three types of mRNAs: mRNAs for which half-lives were stabilized, mRNAs for which half-lives were de-stabilized, and mRNAs bound to PUM1 or PUM2. The intersection of stabilized mRNAs in PUM1 KD cells and PUM1-associating mRNAs were defined as *bona fide* PUM1 target mRNAs.

Figure 3

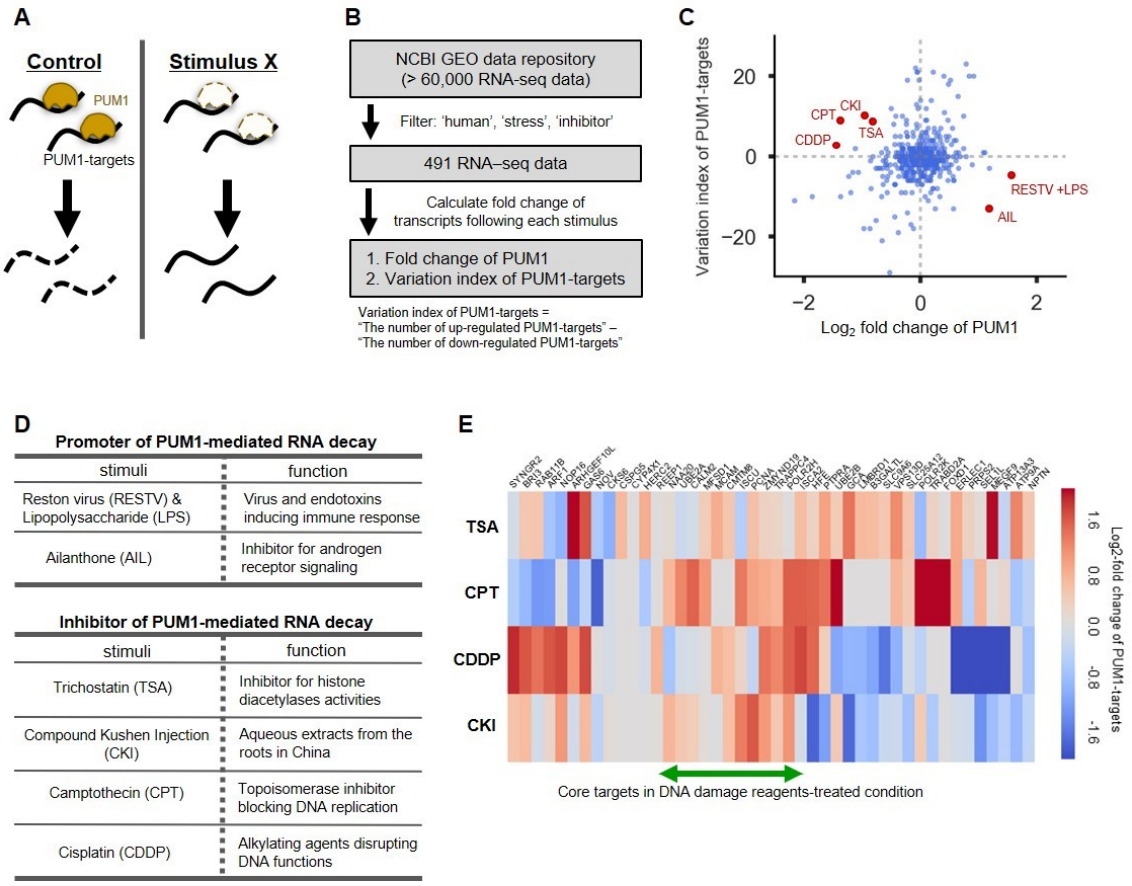

Figure 3. Identification of the stimuli that modulate PUM1-mediated mRNA decay. (A) Basic assumption on *in silico* screening. The stimuli that inversely change PUM1 mRNA and PUM1 targets are candidates of the modulator of PUM1-mediated mRNA decay. (B) Analysis infrastructure to measure the fold change of PUM1 and the variation of PUM1 targets following various stimuli listed in the Gene Expression Omnibus (GEO) repository. (C) Log2-fold change of PUM1 versus Variation index with various stimuli (n = 491). In the panel, the candidate stimuli that modulate PUM1-mediated mRNA decay are highlighted in red dots. (D) List of the stimuli that modulate PUM1-mediated mRNA decay. (E) Heat map of fold-change in the PUM1 targets (48 genes, rows) following indicated stimuli.

Figure 4

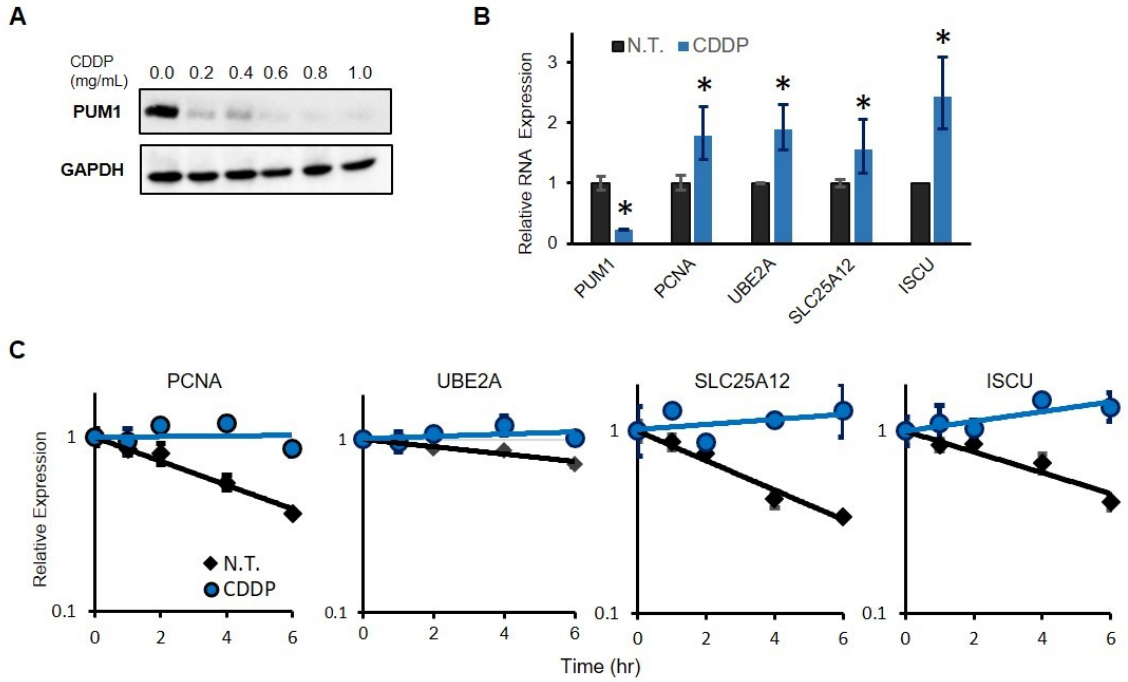

Figure 4. Collapse of PUM1-mediated mRNA decay by CDDP. (A) A Western blot confirming the loss of PUM1 by CDDP treatment. (B) Expression of PUM1 and PUM1-target mRNAs (*PCNA*, *UBE2A*, *SLC25A12*, and *ISCU*) in HeLa cells treated with CDDP. Indicated mRNA levels determined by Real-time RT-qPCR normalized to *GAPDH* and *PGK1* are shown (mean ± SD). *: p value < 0.05 (Student's t-test). (C) Messenger RNA decays of indicated transcripts in HeLa cells treated with CDDP or DMSP (CTRL), followed by actinomycin D chase. Total RNAs were isolated at indicated time points after actinomycin D treatment and relative mRNA abundances (log10-transfomed) over time are plotted (mean ± SD).

Figure 5

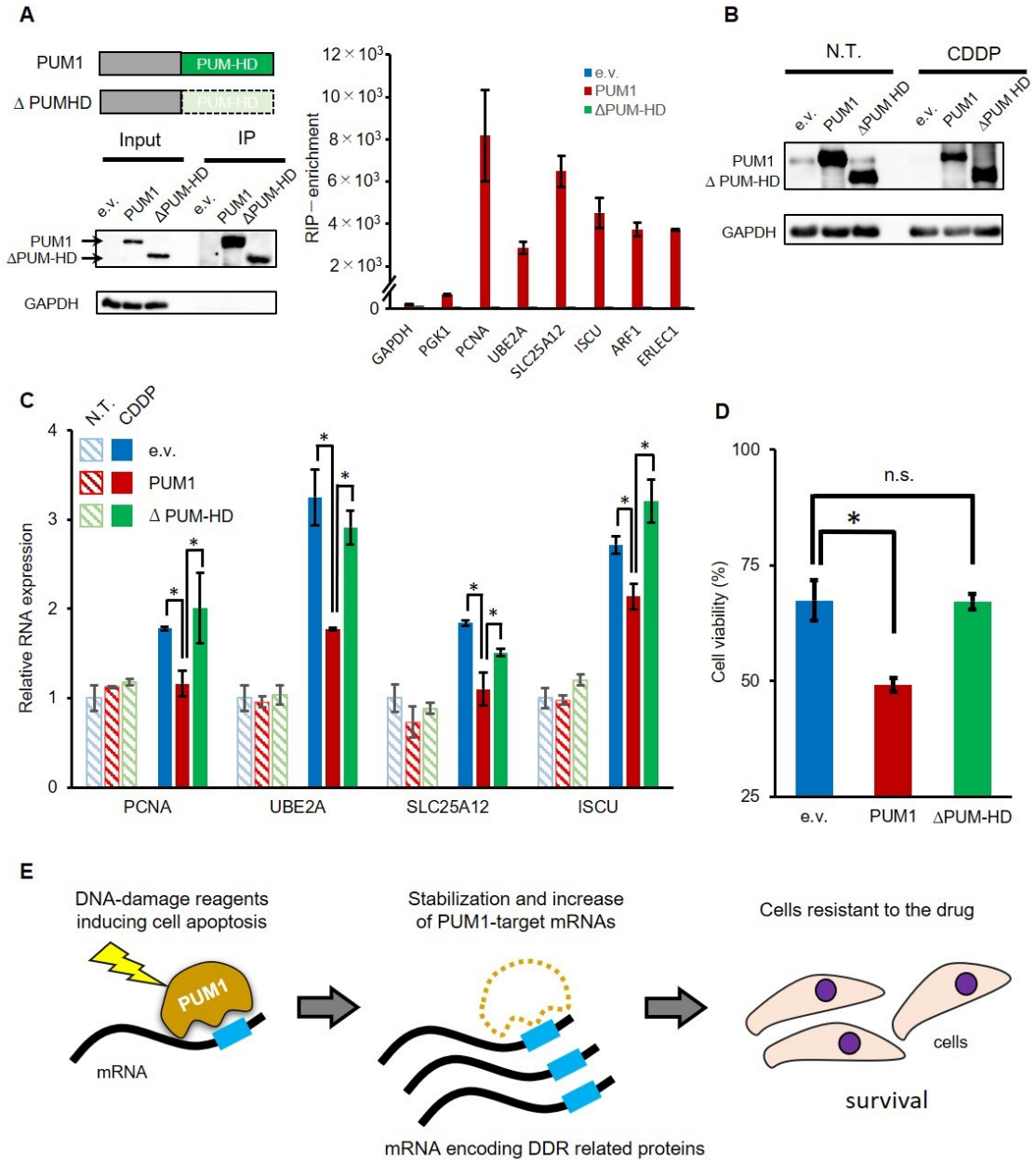

Figure 5. Rescue of endogenous PUM1 decrease by overexpression of exogenous PUM1. (A) RNAs bound to PUM1 or PUM1 deletion mutant of the RNA-binding domain (Δ PUM-HD) were confirmed by RIP followed by real-time RT-qPCR. (B) HeLa cells were transfected with empty vector (e.v.), wild-type PUM1, or PUM1 mutant, which lacks the RNA-binding domain (ΔPUM-HD). The cell lines were treated with 0.5 μg/mL CDDP for 6 hr, followed by Western blot of PUM1 and GAPDH. (C) Real-time RT-qPCR for PUM1 target (*PCNA*, *UBE2A*, *SLC25A12*, and *ISCU*) expression levels in HeLa cells expressing empty vector (e.v.), wild-type PUM1, or Δ PUM-HD after CDDP treatment.

Expression levels of PUM1 targets normalized to *GAPDH* and *PGK1* are shown (mean ± SD). *: p value < 0.05 (Student's t-test). (D) Cell survival of CDDP treated HeLa cells transiently transfected with empty vector (e.v.), wild-type PUM1, or ΔPUM-HD. n.s: not significant ($p \geqq 0.05$). *: p value < 0.05 (Student's t-test). (E) Model of PUM1 function in cell survival to DNA damage agents.

Figure 6

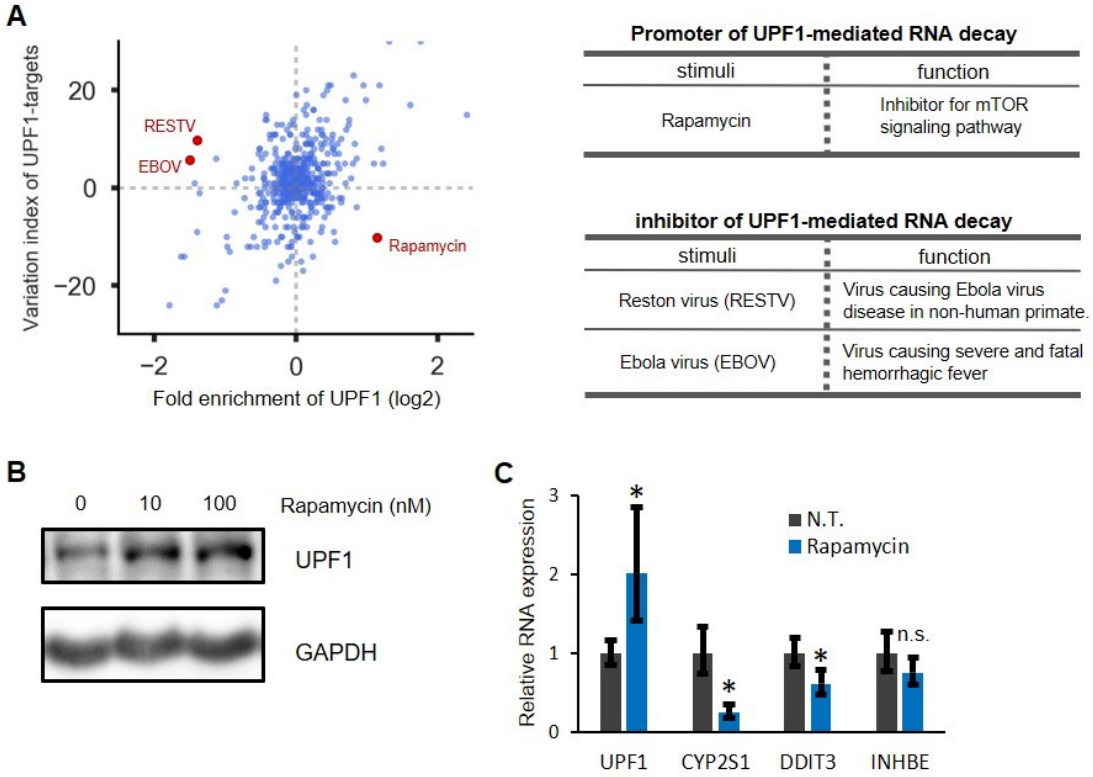

Figure 6. Application of *in silico* screening to UPF1 study. (A) Log2-fold change of UPF1 versus the variation index of UPF1 targets under various stimuli (n = 491). In the scattered plot panel, stimuli that show inverse correlations of UPF1 expression and UPF1 targets are highlighted in red spot. (B) A Western blot confirming the increase of UPF1 by rapamycin. (C) Real-time RT-qPCR to determine the expression of UPF1 and UPF1 targets (*CYP2S1*, *DDIT3*, and *INHBE*) in HEK293 cells treated with rapamycin. The expression levels of the indicated mRNAs were normalized to *SDHA*. n.s: not significant ($p \geqq 0.05$). *: p value < 0.05 (Student's t-test).

1 **Supplemental Information**

Figure S1

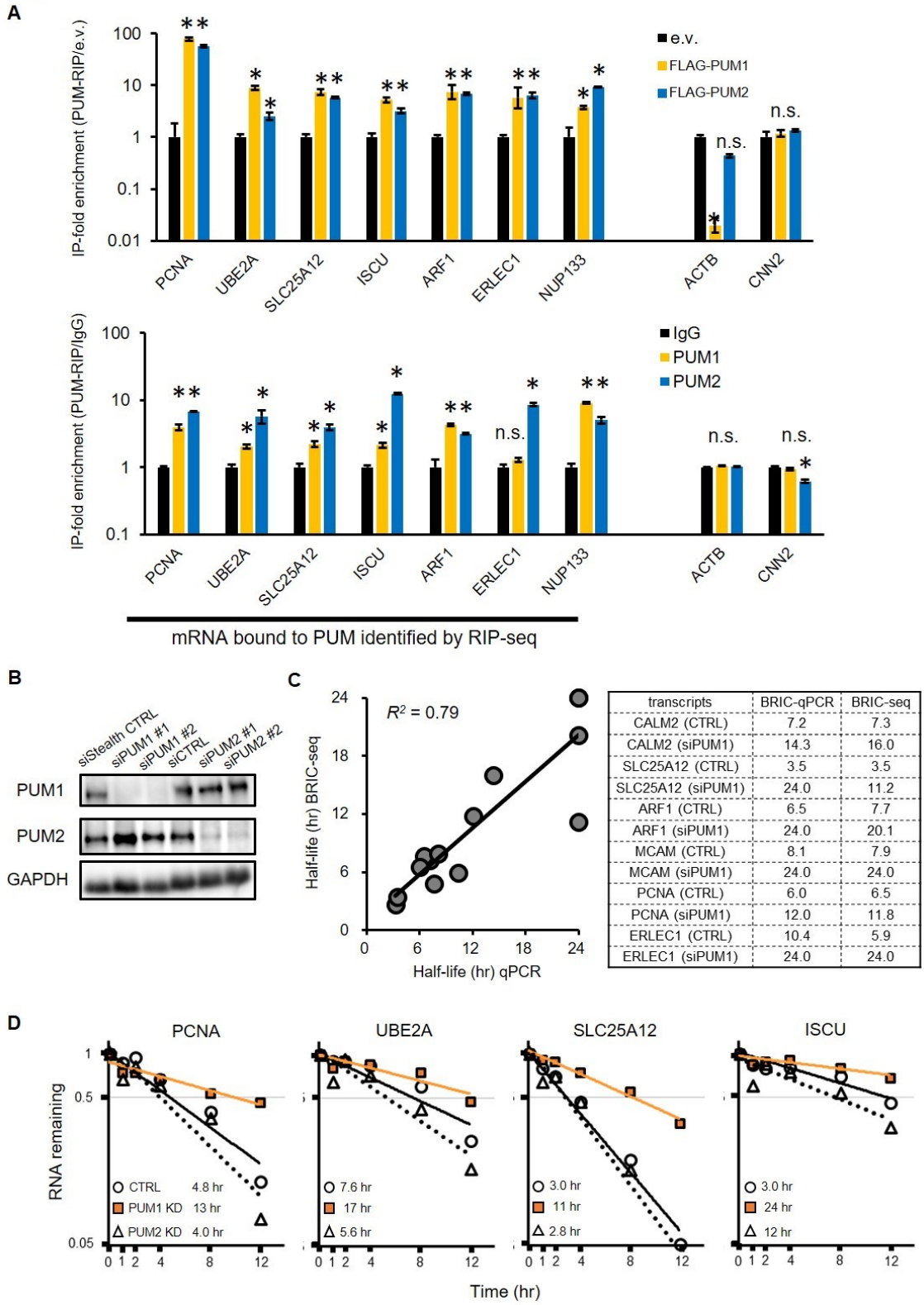

transcripts	BRIC-qPCR	BRIC-seq
CALM2 (CTRL)	7.2	7.3
CALM2 (siPUM1)	14.3	16.0
SLC25A12 (CTRL)	3.5	3.5
SLC25A12 (siPUM1)	24.0	11.2
ARF1 (CTRL)	6.5	7.7
ARF1 (siPUM1)	24.0	20.1
MCAM (CTRL)	8.1	7.9
MCAM (siPUM1)	24.0	24.0
PCNA (CTRL)	6.0	6.5
PCNA (siPUM1)	12.0	11.8
ERLEC1 (CTRL)	10.4	5.9
ERLEC1 (siPUM1)	24.0	24.0

2

3 **Figure S1** (related to **Figure 2**). **Validation of NGS data with qPCR**. (A) RT-qPCR on

mRNA isolated from immunoprecipitation of FLAG-PUMs (upper panel) and immunoprecipitation of endogenous PUMs (lower panel) were performed to calculate the enrichment of mRNA by RIP experiments for 7 PUM-bound mRNAs and 2 non-binding mRNAs. Data are represented as the mean ± SD. n.s: not significant ($p \geqq 0.05$). *: p value < 0.05 (Student's t-test). (B) Representative Western blots of PUM1, PUM2, and GAPDH from HeLa cells treated with indicated siRNA. (C) A scatter plot showing the correlation of half-lives of indicated mRNAs determined by BRIC-seq against those calculated by RT-qPCR. (D) Decay plots of mRNAs (PCNA, UBE2A, SLC25A12, and ISCU) determined by BRIC-seq. mRNA decays were calculated with the cells treated with siRNA targeting control (circle), PUM1 (square, yellow), or PUM2 (triangle). In each decay plot, data were curve fitted with the exponential function (solid (CTRL: black and PUM1 KD: yellow) and dashed line (PUM2 KD)).

Figure S2

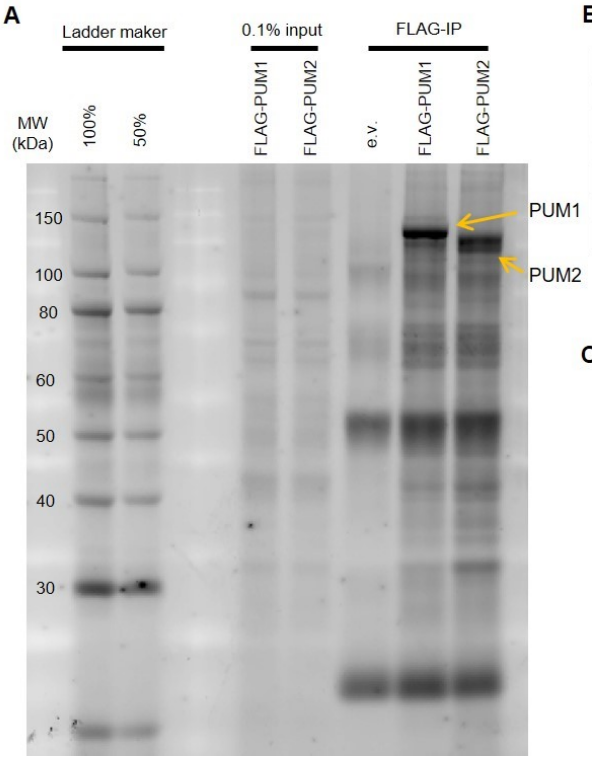

B

Gene	IP-PUM1/IP-PUM2	IP-PUM1/IP-e.v.	IP-PUM2/IP-e.v.
CNOT1	0.9	29	31
CNOT2	1.2	6	5
CNOT7	1.3	8	6
CNOT9	2.7	8	3
EDC4	0.7	6	9
TNRC6A	—	0	5

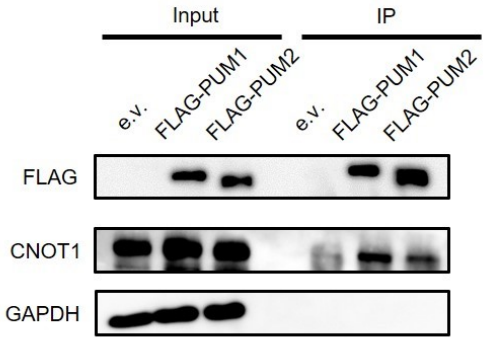

Figure S2 (related to **Figure 2**). **Identification of PUM-associated proteins using Co-IP followed by mass spectrometry**. (A) SDS-PAGE analysis of proteins co-immunoprecipitated with FLAG-PUM1 or FLAG-PUM2. Immunoprecipitants were separated on an SDS gradient gel and visualized by SYPRO Ruby staining. (B) Mass spectrometry analysis showing that RNA degradation factors were co-immunoprecipitated with FLAG-tagged PUM1 or PUM2. The ratios of spectral counts between immunoprecipitated (IPed) fragment with PUM1 (IP-PUM1) versus Iped fragment with PUM2 (IP-PUM2), IP-PUM1 versus Iped fragment with empty vector (IP-e.v.), and IP-PUM2 versus IP-e.v. are shown. A complete list of the interacting proteins is provided in **Table S5**. (C) Co-immunoprecipitation of PUMs and CNOT1. The input corresponds to 20%. GAPDH served as negative control.

Figure S3

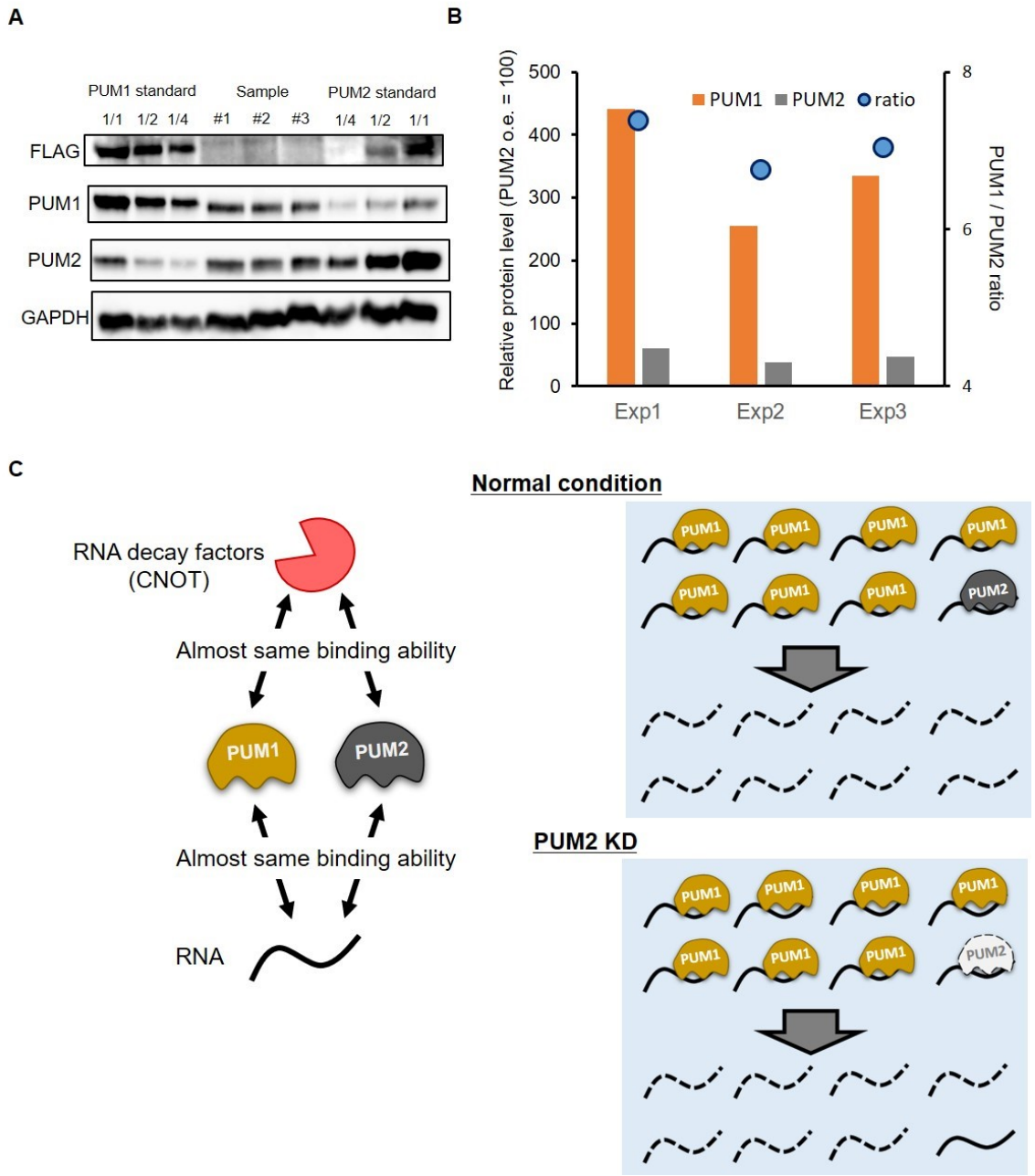

Figure S3 (related to **Figure 2**). **Quantitative comparison of PUM1/PUM2 ratio**. (A) Endogenous and exogenous PUM protein levels analyzed by Western blot using indicated antibody in biological triplicates (indicated as "Sample"). GAPDH was used as normalizer for the number of cells in each sample. Among the standard samples, 1/1, 1/2, and 1/4 indicate dilution factors. (B) Orange and gray bars indicate relative protein levels (left vertical line) of PUM1 and PUM2 in sample cell #1 - #3 (biological triplicates) of (A), respectively. Here, the signal intensity of PUM2 overexpression (PUM2 o.e.) was set

at 100. Blue circles (right vertical line) show the ratio of PUM1/PUM2 in each sample.
(C) Model of dominant PUM1-mediated mRNA decay in HeLa TO cells.

Figure S4

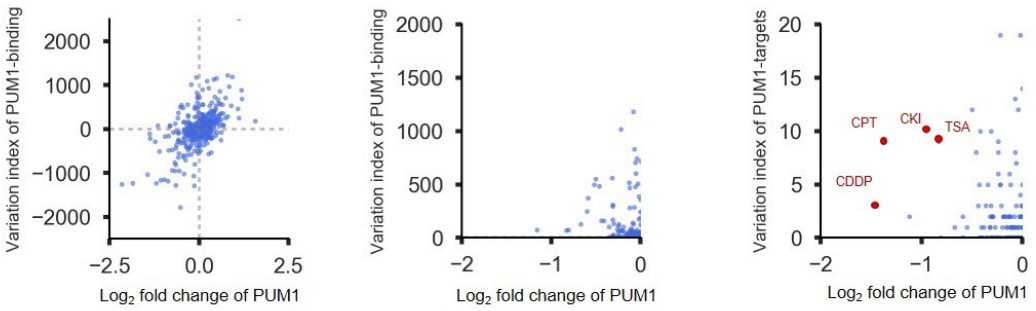

Figure S4 (related to **Figure 3**) ***In silico* screening on PUM1-bound mRNAs.** Log2-fold change of PUM1 versus Variation index calculated from 3,097 PUM1-binding mRNAs following various stimuli (n = 491). An enlarged figure of the second quadrant is shown in the middle panel. For comparison, the second quadrant of **Figure 3D** is also shown in the right panel.

Figure S5

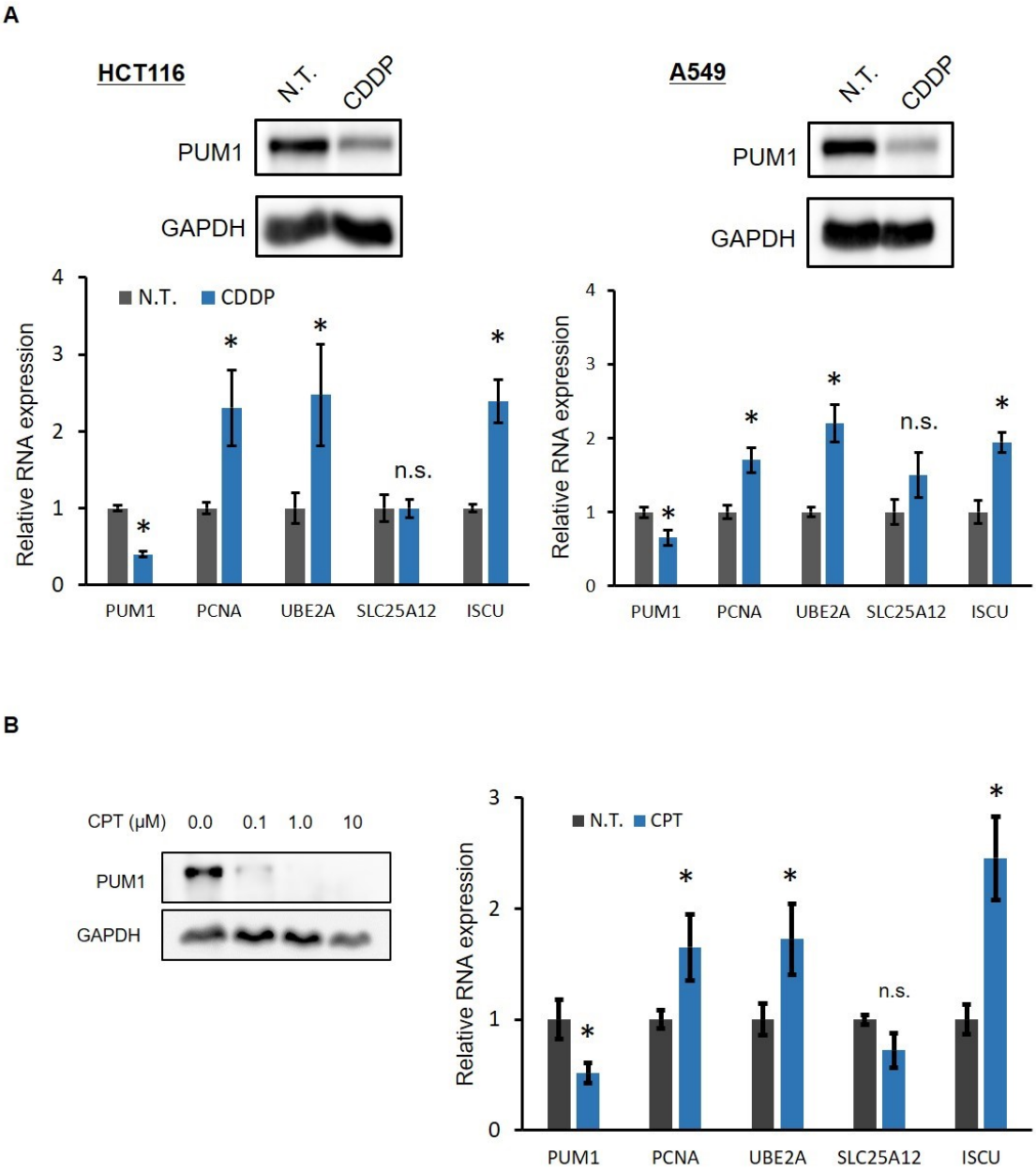

Figure S5 (related to **Figure 4**) **Collapse of PUM1-mediated mRNA decay by CDDP in HCT116 and A549 cells (A) and camptothecin (CPT) in HeLa cells (B)**. In each condition, Western blots confirmed the depletion of PUM1. Real-time RT-qPCR determined the expression level of indicated mRNAs in indicated cells treated with CDDP (A) or CPT (B). Each mRNA expression was normalized to *GAPDH* and *PGK1* (mean ± SD). n.s.: not significant ($p \geqq 0.05$). *: p value < 0.05 (Student's t-test).

References

Arif, A., Jia, J., Mukhopadhyay, R., Willard, B., Kinter, M., and Fox, P.L. (2009). Two-Site Phosphorylation of EPRS Coordinates Multimodal Regulation of Noncanonical Translational Control Activity. Mol. Cell *35*, 164–180.

Bar-Joseph, Z., Gerber, G.K., Lee, T.I., Rinaldi, N.J., Yoo, J.Y., Robert, F., Gordon, D.B., Fraenkel, E., Jaakkola, T.S., Young, R.A., et al. (2003). Computational discovery of gene modules and regulatory networks. Nat. Biotechnol. *21*, 1337–1342.

Chen, D., Zheng, W., Lin, A., Uyhazi, K., Zhao, H., and Lin, H. (2012). Pumilio 1 Suppresses Multiple Activators of p53 to Safeguard Spermatogenesis. Curr. Biol. *22*, 420–425.

Curtin, N.J. (2012). DNA repair dysregulation from cancer driver to therapeutic target. Nat. Rev. Cancer *12*, nrc3399.

Dominguez, D., Freese, P., Alexis, M.S., Su, A., Hochman, M., Palden, T., Bazile, C., Lambert, N.J., Van Nostrand, E.L., Pratt, G.A., et al. (2018). Sequence, Structure, and Context Preferences of Human RNA Binding Proteins. Mol. Cell *70*, 854–867.e9.

Elkayam, E., Faehnle, C.R., Morales, M., Sun, J., Li, H., and Joshua-Tor, L. (2017). Multivalent Recruitment of Human Argonaute by GW182. Mol. Cell *67*, 646–658.e3.

Etten, J. Van, Schagat, T.L., Hrit, J., Weidmann, C.A., Brumbaugh, J., Coon, J.J., and Goldstrohm, A.C. (2012). Human Pumilio Proteins Recruit Multiple Deadenylases to Efficiently Repress Messenger RNAs. J. Biol. Chem. *287*, 36370–36383.

Favaro, E., Ramachandran, A., McCormick, R., Gee, H., Blancher, C., Crosby, M., Devlin, C., Blick, C., Buffa, F., Li, J.-L., et al. (2010). MicroRNA-210 Regulates Mitochondrial Free Radical Response to Hypoxia and Krebs Cycle in Cancer Cells by Targeting Iron Sulfur Cluster Protein ISCU. PLoS One *5*, e10345.

Galgano, A., Forrer, M., Jaskiewicz, L., Kanitz, A., Zavolan, M., and Gerber, A.P. (2008). Comparative Analysis of mRNA Targets for Human PUF-Family Proteins Suggests Extensive Interaction with the miRNA Regulatory System. PLoS One *3*, e3164.

García-Rodríguez, L.J., Gay, A.C., and Pon, L.A. (2007). Puf3p, a Pumilio family RNA binding protein, localizes to mitochondria and regulates mitochondrial biogenesis and motility in budding yeast. J. Cell Biol. *176*, 197–207.

Gardner, T.S., Bernardo, D. di, Lorenz, D., and Collins, J.J. (2003). Inferring Genetic Networks and Identifying Compound Mode of Action via Expression Profiling. Science (80-.). *301*, 102–105.

Gerber, A.P., Herschlag, D., and Brown, P.O. (2004). Extensive Association of Functionally and Cytotopically Related mRNAs with Puf Family RNA-Binding

Proteins in Yeast. PLoS Biol. *2*, e79.
Giglia-Mari, G., Zotter, A., and Vermeulen, W. (2011). DNA damage response. Cold Spring Harb. Perspect. Biol. *3*, a000745.
Hafner, M., Landthaler, M., Burger, L., Khorshid, M., Hausser, J., Berninger, P., Rothballer, A., Ascano, M., Jungkamp, A.-C., Munschauer, M., et al. (2010). Transcriptome-wide Identification of RNA-Binding Protein and MicroRNA Target Sites by PAR-CLIP. Cell *141*, 129–141.
He, Y., Peng, S., Wang, J., Chen, H., Cong, X., Chen, A., Hu, M., Qin, M., Wu, H., Gao, S., et al. (2016). Ailanthone targets p23 to overcome MDV3100 resistance in castration-resistant prostate cancer. Nat. Commun. *7*, ncomms13122.
Hentze, M.W., Castello, A., Schwarzl, T., and Preiss, T. (2018). A brave new world of RNA-binding proteins. Nat. Rev. Mol. Cell Biol.
Hoege, C., Pfander, B., Moldovan, G.-L., Pyrowolakis, G., and Jentsch, S. (2002). RAD6-dependent DNA repair is linked to modification of PCNA by ubiquitin and SUMO. Nature *419*, 135–141.
Housman, G., Byler, S., Heerboth, S., Lapinska, K., Longacre, M., Snyder, N., and Sarkar, S. (2014). Drug Resistance in Cancer: An Overview. Cancers (Basel). *6*, 1769–1792.
Hu, Z., Killion, P.J., and Iyer, V.R. (2007). Genetic reconstruction of a functional transcriptional regulatory network. Nat. Genet. *39*, 683–687.
Imamachi, N., Tani, H., and Akimitsu, N. (2012). Up-frameshift protein 1 (UPF1): multitalented entertainer in RNA decay. Drug Discov. Ther. *6*, 55–61.
Imamachi, N., Salam, K.A., Suzuki, Y., and Akimitsu, N. (2016). A GC-rich sequence feature in the 3′ UTR directs UPF1-dependent mRNA decay in mammalian cells. Genome Res. *27*, 407–418.
Isken, O., and Maquat, L.E. (2007). Quality control of eukaryotic mRNA: safeguarding cells from abnormal mRNA function. Genes Dev. *21*, 1833–3856.
Jakymiw, A., Lian, S., Eystathioy, T., Li, S., Satoh, M., Hamel, J.C., Fritzler, M.J., and Chan, E.K.L. (2005). Disruption of GW bodies impairs mammalian RNA interference. Nat. Cell Biol. *7*, 1267–1274.
Karlebach, G., and Shamir, R. (2008). Modelling and analysis of gene regulatory networks. Nat. Rev. Mol. Cell Biol. *9*, nrm2503.
Kaye, J.A., Rose, N.C., Goldsworthy, B., Goga, A., and L'Etoile, N.D. (2009). A 3'UTR pumilio-binding element directs translational activation in olfactory sensory neurons. Neuron *61*, 57–70.
Kedde, M., Kouwenhove, M. van, Zwart, W., Vrielink, J.A.F.O., Elkon, R., and Agami,

R. (2010). A Pumilio-induced RNA structure switch in p27-3′ UTR controls miR-221 and miR-222 accessibility. Nat. Cell Biol. *12*, 1014–1020.

Keene, J.D. (2007). RNA regulons: coordination of post-transcriptional events. Nat. Rev. Genet. *8*, 533–543.

Lambert, N., Robertson, A., Jangi, M., McGeary, S., Sharp, P.A., and Burge, C.B. (2014). RNA Bind-n-Seq: Quantitative Assessment of the Sequence and Structural Binding Specificity of RNA Binding Proteins. Mol. Cell *54*, 887–900.

Lee, S., Kopp, F., Chang, T.-C., Sataluri, A., Chen, B., Sivakumar, S., Yu, H., Xie, Y., and Mendell, J.T. (2016). Noncoding RNA NORAD Regulates Genomic Stability by Sequestering PUMILIO Proteins. Cell *164*, 69–80.

Lee, T.I., Rinaldi, N.J., Robert, F., Odom, D.T., Bar-Joseph, Z., Gerber, G.K., Hannett, N.M., Harbison, C.T., Thompson, C.M., Simon, I., et al. (2002). Transcriptional Regulatory Networks in Saccharomyces cerevisiae. Science (80-.). *298*, 799–804.

López-Maury, L., Marguerat, S., and Bähler, J. (2008). Tuning gene expression to changing environments: from rapid responses to evolutionary adaptation. Nat. Rev. Genet. *9*, 583–593.

Lord, C.J., and Ashworth, A. (2012). The DNA damage response and cancer therapy. Nature *481*, 287–294.

Maquat, L.E. (2004). Nonsense-mediated mRNA decay: splicing, translation and mRNP dynamics. Nat. Rev. Mol. Cell Biol. *5*, nrm1310.

Martinez-Nunez, R.T., Wallace, A., Coyne, D., Jansson, L., Rush, M., Ennajdaoui, H., Katzman, S., Bailey, J., Deinhardt, K., Sanchez-Elsner, T., et al. (2017). Modulation of nonsense mediated decay by rapamycin. Nucleic Acids Res. *45*, 3448–3459.

Miller, M.A., and Olivas, W.M. (2011). Roles of Puf proteins in mRNA degradation and translation. Wiley Interdiscip. Rev. RNA *2*, 471–492.

Miller, C., Schwalb, B., Maier, K., Schulz, D., Dümcke, S., Zacher, B., Mayer, A., Sydow, J., Marcinowski, L., Dölken, L., et al. (2011). Dynamic transcriptome analysis measures rates of mRNA synthesis and decay in yeast. Mol. Syst. Biol. *7*, 458.

Moldovan, G.-L., Pfander, B., and Jentsch, S. (2007). PCNA, the Maestro of the Replication Fork. Cell *129*, 665–679.

Morris, A.R., Mukherjee, N., and Keene, J.D. (2008). Ribonomic Analysis of Human Pum1 Reveals cis-trans Conservation across Species despite Evolution of Diverse mRNA Target Sets. Mol. Cell. Biol. *28*, 4093–4103.

Mukhopadhyay, R., Ray, P.S., Arif, A., Brady, A.K., Kinter, M., and Fox, P.L. (2008). DAPK-ZIPK-L13a Axis Constitutes a Negative-Feedback Module Regulating Inflammatory Gene Expression. Mol. Cell *32*, 371–382.

Nadal, E. de, Ammerer, G., and Posas, F. (2011). Controlling gene expression in response to stress. Nat. Rev. Genet. *12*, 833–845.

Narita, R., Takahasi, K., Murakami, E., Hirano, E., Yamamoto, S.P., Yoneyama, M., Kato, H., and Fujita, T. (2014). A Novel Function of Human Pumilio Proteins in Cytoplasmic Sensing of Viral Infection. PLoS Pathog. *10*, e1004417.

Nasif, S., Contu, L., and Mühlemann, O. (2018). Beyond quality control: The role of nonsense-mediated mRNA decay (NMD) in regulating gene expression. Semin. Cell Dev. Biol. *75*, 78–87.

Nishi, K., Nishi, A., Nagasawa, T., and Ui-Tei, K. (2013). Human TNRC6A is an Argonaute-navigator protein for microRNA-mediated gene silencing in the nucleus. RNA *19*, 17–35.

Nostrand, E.L. Van, Pratt, G.A., Shishkin, A.A., Gelboin-Burkhart, C., Fang, M.Y., Sundararaman, B., Blue, S.M., Nguyen, T.B., Surka, C., Elkins, K., et al. (2016). Robust transcriptome-wide discovery of RNA-binding protein binding sites with enhanced CLIP (eCLIP). Nat. Methods *13*, nmeth.3810.

Nussbacher, J.K., and Yeo, G.W. (2018). Systematic Discovery of RNA Binding Proteins that Regulate MicroRNA Levels. Mol. Cell *69*, 1005–1016.e7.

O'Connor, M.J. (2015). Targeting the DNA Damage Response in Cancer. Mol. Cell *60*, 547–560.

Pearl, L.H., Schierz, A.C., Ward, S.E., Al-Lazikani, B., and Pearl, F.M.G. (2015). Therapeutic opportunities within the DNA damage response. Nat. Rev. Cancer *15*, 166–180.

Qu, Z., Cui, J., Harata-Lee, Y., Aung, T.N., Feng, Q., Raison, J.M., Kortschak, R.D., and Adelson, D.L. (2016). Identification of candidate anti-cancer molecular mechanisms of compound kushen injection using functional genomics. Oncotarget *7*, 66003–66019.

Quenault, T., Lithgow, T., and Traven, A. (2011). PUF proteins: repression, activation and mRNA localization. Trends Cell Biol. *21*, 104–112.

Rabani, M., Levin, J.Z., Fan, L., Adiconis, X., Raychowdhury, R., Garber, M., Gnirke, A., Nusbaum, C., Hacohen, N., Friedman, N., et al. (2011). Metabolic labeling of RNA uncovers principles of RNA production and degradation dynamics in mammalian cells. Nat. Biotechnol. *29*, 436–442.

Rabani, M., Raychowdhury, R., Jovanovic, M., Rooney, M., Stumpo, D.J., Pauli, A., Hacohen, N., Schier, A.F., Blackshear, P.J., Friedman, N., et al. (2014). High-Resolution Sequencing and Modeling Identifies Distinct Dynamic RNA Regulatory Strategies. Cell *159*, 1698–1710.

Roos, W.P., and Kaina, B. (2006). DNA damage-induced cell death by apoptosis. Trends Mol. Med. *12*, 440–450.

Roos, W.P., and Kaina, B. (2013). DNA damage-induced cell death: From specific DNA lesions to the DNA damage response and apoptosis. Cancer Lett. *332*, 237–248.

Rudolf, J., Makrantoni, V., Ingledew, W.J., Stark, M.J.R., and White, M.F. (2006). The DNA repair helicases XPD and FancJ have essential iron-sulfur domains. Mol. Cell *23*, 801–808.

Sanders, M.A., Haynes, B., Nangia-Makker, P., Polin, L.A., and Shekhar, M.P. (2017). Pharmacological targeting of RAD6 enzyme-mediated translesion synthesis overcomes resistance to platinum-based drugs. J. Biol. Chem. *292*, 10347–10363.

Schweingruber, C., Rufener, S.C., Zünd, D., Yamashita, A., and Mühlemann, O. (2013). Nonsense-mediated mRNA decay — Mechanisms of substrate mRNA recognition and degradation in mammalian cells. Biochim. Biophys. Acta - Gene Regul. Mech. *1829*, 612–623.

Segal, E., Shapira, M., Regev, A., Pe'er, D., Botstein, D., Koller, D., and Friedman, N. (2003). Module networks: identifying regulatory modules and their condition-specific regulators from gene expression data. Nat. Genet. *34*, 166–176.

Somasagara, R.R., Spencer, S.M., Tripathi, K., Clark, D.W., Mani, C., Madeira da Silva, L., Scalici, J., Kothayer, H., Westwell, A.D., Rocconi, R.P., et al. (2017). RAD6 promotes DNA repair and stem cell signaling in ovarian cancer and is a promising therapeutic target to prevent and treat acquired chemoresistance. Oncogene *36*, 6680–6690.

Spassov, D.S., and Jurecic, R. (2002). Cloning and comparative sequence analysis of PUM1 and PUM2 genes, human members of the Pumilio family of RNA-binding proteins. Gene *299*, 195–204.

Spriggs, K.A., Bushell, M., and Willis, A.E. (2010). Translational Regulation of Gene Expression during Conditions of Cell Stress. Mol. Cell *40*, 228–237.

Stoimenov, I., and Helleday, T. (2009). PCNA on the crossroad of cancer. Biochem. Soc. Trans. *37*, 605–613.

Sundararaman, B., Zhan, L., Blue, S.M., Stanton, R., Elkins, K., Olson, S., Wei, X., Van Nostrand, E.L., Pratt, G.A., Huelga, S.C., et al. (2016). Resources for the Comprehensive Discovery of Functional RNA Elements. Mol. Cell *61*, 903–913.

Tani, H., Mizutani, R., Salam, K.A., Tano, K., Ijiri, K., Wakamatsu, A., Isogai, T., Suzuki, Y., and Akimitsu, N. (2012). Genome-wide determination of RNA stability reveals hundreds of short-lived noncoding transcripts in mammals. Genome Res. *22*, 947–956.

Tong, W.-H., and Rouault, T.A. (2006). Functions of mitochondrial ISCU and cytosolic ISCU in mammalian iron-sulfur cluster biogenesis and iron homeostasis. Cell Metab. *3*, 199–210.

Vessey, J.P., Vaccani, A., Xie, Y., Dahm, R., Karra, D., Kiebler, M.A., and Macchi, P. (2006). Dendritic Localization of the Translational Repressor Pumilio 2 and Its Contribution to Dendritic Stress Granules. J. Neurosci. *26*, 6496–6508.

Vessey, J.P., Schoderboeck, L., Gingl, E., Luzi, E., Riefler, J., Leva, F. Di, Karra, D., Thomas, S., Kiebler, M.A., and Macchi, P. (2010). Mammalian Pumilio 2 regulates dendrite morphogenesis and synaptic function. Proc. Natl. Acad. Sci. *107*, 3222–3227.

Wang, S.-C. (2014). PCNA: a silent housekeeper or a potential therapeutic target? Trends Pharmacol. Sci. *35*, 178–186.

Wang, M., Ogé, L., Perez-Garcia, M.-D., Hamama, L., and Sakr, S. (2018). The PUF Protein Family: Overview on PUF RNA Targets, Biological Functions, and Post Transcriptional Regulation. Int. J. Mol. Sci. *19*, 410.

Wang, W., You, R., Qin, W., Hai, L., Fang, M., Huang, G., Kang, R., Li, M., Qiao, Y., Li, J., et al. (2015). Anti-tumor activities of active ingredients in Compound Kushen Injection. Acta Pharmacol. Sin. *36*, aps201524.

Wang, X., Zamore, P.D., and Hall, T.M.T. (2001). Crystal Structure of a Pumilio Homology Domain. Mol. Cell *7*, 855–865.

Wang, X., McLachlan, J., Zamore, P.D., and Hall, T.M.T. (2002). Modular Recognition of RNA by a Human Pumilio-Homology Domain. Cell *110*, 501–512.

Wheeler, E.C., Van Nostrand, E.L., and Yeo, G.W. (2018). Advances and challenges in the detection of transcriptome-wide protein-RNA interactions. Wiley Interdiscip. Rev. RNA *9*, e1436.

Wickens, M., Bernstein, D.S., Kimble, J., and Parker, R. (2002). A PUF family portrait: 3′UTR regulation as a way of life. Trends Genet. *18*, 150–157.

Yamada, T., Imamachi, N., Onoguchi-Mizutani, R., Imamura, K., Suzuki, Y., and Akimitsu, N. (2018). 5′-Bromouridine IP Chase (BRIC)-Seq to Determine RNA Half-Lives. In Methods in Molecular Biology (Clifton, N.J.), pp. 1–13.

Zhang, H., and Yu, D.S. (2012). One stone, two birds. Cell Cycle *11*, 2418–2418.

Zhao, J., Ohsumi, T.K., Kung, J.T., Ogawa, Y., Grau, D.J., Sarma, K., Song, J.J., Kingston, R.E., Borowsky, M., and Lee, J.T. (2010). Genome-wide Identification of Polycomb-Associated RNAs by RIP-seq. Mol. Cell *40*, 939–953.